(1)

AD A136922

AIR FORCE INSTITUTE OF TECHNOLOGY

AIR UNIVERSITY
UNITED STATES AIR FORCE

TRANSITION OF CORNER CRACKS AT HOLES INTO

THROUGH-THE-THICKNESS CRACKS

THESIS

Stephen W. Opel
Captain, USAF

AFIT/GAE/AA/83D-17

SCHOOL OF ENGINEERING

DTIC
ELECTE
JAN 17 1984
S D

WRIGHT-PATTERSON AIR FORCE BASE, OHIO

DTIC FILE COPY

84 01 17 077

This document has been approved for public release and sale; its distribution is unlimited.

AFIT/GAE/AA/83D-17

TRANSITION OF CORNER CRACKS AT HOLES INTO

THROUGH-THE-THICKNESS CRACKS

THESIS

Stephen W. Opel
Captain, USAF

AFIT/GAE/AA/83D-17

Approved for public release; distribution unlimited

AFIT/GAE/AA/83D-17

TRANSITION OF CORNER CRACKS AT HOLES INTO THROUGH-THE-THICKNESS CRACKS

THESIS

Presented to the Faculty of the School of Engineering

of the Air Force Institute of Technology

Air University

In Partial Fulfillment of the

Requirements for the Degree of

Master of Science in Aeronautical Engineering

Stephen W. Opel, B.S.

Captain, USAF

December 1983

Accession For

Availability Codes

Avail and/or

Dist Special

A-1

DTIC COPY INSPECTED 2

Approved for public release; distribution unlimited

TABLE of CONTENTS

	Page
Acknowledgements	iv
List of Figures	v
List of Tables	ix
Abstract	x
I. Introduction	1
Motivation	1
Background	2
Stress Intensity Factors for Corner Cracks Emanating from a Hole	2
Transition of a Corner Crack at a Hole to a Through-the-Thickness Crack	5
Problem Statement	7
Objectives	7
Approach	9
II. Testing	11
Polymethylmethacrylate (PMMA) Testing	11
Crack Growth Rate Tests	11
Corner-Crack-at-a-Hole-Tests	11
7075-T651 Aluminum Testing	16
Crack Growth Rate Tests	16
Corner-Crack-at-a-Hole Tests	18
Corner-Crack to Final Fracture Tests	22
III. Experimental Stress Intensity Factors	23
Corner-Crack-at-a-Hole Until Back Surface Penetration	23
Back Surface Penetration Until Final Fracture	25

IV. Analytical Stress Intensity Factors..... 27

Analytical Solution Used for the Corner Crack..... 27

Analytical Solution Used for the Through-Crack..... 28

V. Analytical/Experimental Correlations..... 29

Corner Crack Until Back Surface Penetration..... 29

Back Surface Penetration Until Final Fracture..... 38

VI. Correction Factor Development..... 42

Corner Crack Until Back Surface Penetration Region..... 42

Correction for Stress Intensity Factor Along the Bore of the Hole..... 42

Correction for the Stress Intensity Factor Along the Front Surface..... 45

Back Surface Penetration Until Final Fracture Region.... 53

Correction for Stress Intensity Factor Along the Back Surface..... 53

Correction for Stress Intensity Factor Along the Front Surface..... 56

Back Surface Crack Length as a Function of Front Surface Crack Length..... 56

VII. Life and Crack Shape Predictions and Comparisons..... 60

Life Predictions Based Upon Corrected Stress Intensity Factors..... 60

Life Predictions Based On Other Models..... 62

Newman-Bowie Method..... 62

Brussat Method..... 62

Crack Shape Predictions..... 64

Comparisons..... 67

VIII. Conclusions and Recommendations..... 70

Appendix: Crack Growth Rate Plots..... 72

Bibliography..... 87

Vita..... 90

Acknowledgements

I would like to express my appreciation to Mr. James L. Rudd, and the Fatigue and Fracture Branch of the Air Force Wright Aeronautical Laboratories, who were the sponsors of this research. Without Mr. Rudd's guidance and the hours of discussion regarding this work, the results of this study would not have been attained. Additionally, the support and counsel of my advisor, Major George K. Haritos, was essential to the preparation of this thesis. Last, but surely not least, a special note of thanks is due to my wife, Robin, for her support in typing this thesis, her encouragement, and understanding during the course of this work.

List of Figures

Figure		Page
1	Crack Configurations as it Transitions from a Corner Crack to a Through-the-Thickness Crack	8
2	Schematic of Tests Conducted by Grandt and Hinnerichs	12
3	Specimen Geometry Used by Grandt and Snow	13
4	Center-Crack-Tension Specimen Geometry Used by Heckel and Rudd	17
5	Specimen Geometry Used for 7075-T651 Aluminum Testing	19
6	Schematic of James-Anderson Backtracking Technique	24
7	Correlation of Stress Intensity Factors Along the Bore of the Hole for PMMA Tests	34
8	Correlation of Stress Intensity Factors Along the Bore of the Hole for PMMA Tests (Expanded y-axis)	35
9	Correlation of Stress Intensity Factors Along the Front Surface of the PMMA Tests	36
10	Correlation of Stress Intensity Factors Along the Front Surface of the PMMA Tests (Expanded y-axis)	37
11	Correlation of Stress Intensity Factors Along the Back Surface of the 7075-T651 Aluminum Tests Until Normalized Crack Length Equals 2.5	39
12	Correlation of Stress Intensity Factors Along the Front Surface of the 7075-T651 Aluminum Tests Until Normalized Crack Length Equals 2.5	41
13	Correlation of Stress Intensity Factors Along the Bore of the Hole in the Region of Interest (Correction Factor Plotted in Transition Region)	43
14	Correlation of Stress Intensity Factors Along the Bore of the Hole in the Region of Interest (Correction Factor Plotted in Transition Region) (Expanded y-axis)	44
15	Correlation of Stress Intensity Factors Along the Bore of the Hole in the Region of Interest after Applying the Correction Factor (Best Fit Linear Function Plotted in Transition Region)	46

Figure		Page
16	Correction of Stress Intensity Factors Along the Bore of the Hole in the Region of Interest after Applying the Correction Factor (Best Fit Linear Function Plotted in Transition Region) (Expanded y-axis).....	47
17	Correlation of Stress Intensity Factors Along the Entire Length of the Bore of the Hole (Best Fit Linear Function Plotted for Entire Region).....	48
18	Correlation of Stress Intensity Factors Along the Front Surface of the PMMA Tests in the Region of Interest (Correction Factor Plotted in Transition Region).....	49
19	Correlation of Stress Intensity Factors Along the Front Surface of the PMMA Tests in the Region of Interest (Correction Factor Plotted in Transition Region) (Expanded y-axis).....	50
20	Correlation of Stress Intensity Factors Along the Front Surface of the PMMA Tests in the Region of Interest After Applying the Correction Factor (Best Fit Linear Function Plotted in Transition Region).....	51
21	Correlation of Stress Intensity Factors Along the Front Surface of the PMMA Tests in the Region of Interest After Applying the Correction Factor (Best Fit Linear Function Plotted in Transition Region) (Expanded y-axis)	52
22	Correlation of Stress Intensity Factors Along the Front Surface of the PMMA Tests After Applying the Correction Factor (Best Fit Linear Function Plotted for Entire Region).....	54
23	Correlation of Stress Intensity Factors Along the Back Surface of the 7075-T651 Aluminum Tests in the Region of Interest (Correction Factor Plotted in Transition Region).....	55
24	Correlation of Stress Intensity Factors Along the Front Surface of the 7075-T651 Aluminum Tests in the Region of Interest (Correction Factor Plotted in Transition Region).....	57
25	Relationship of the Normalized Back Surface Crack Length as a Function of the Normalized Front Surface Crack Length (Best Fit Relationship Plotted).....	58
26	Percent of Life Predicted by Corrected Model and by Newman-Raju Model in the Transition Region at Specific Points.....	68

Figure		Page
A-1	Crack Growth Rate for the Back Surface of 7075-T651 Aluminum Specimens with a Maximum Stress of 20 and a Load Ratio of 0.1 as a Function of Crack Length.....	73
A-2	Crack Growth Rate for the Back Surface of 7075-T651 Aluminum Specimens with a Maximum Stress of 15 and a Load Ratio of 0.1 as a Function of Crack Length.....	74
A-3	Crack Growth Rate for the Back Surface of 7075-T651 Aluminum Specimens with a Maximum Stress of 20 and a Load Ratio of 0.3 as a Function of Crack Length.....	75
A-4	Crack Growth Rate for the Back Surface of 7075-T651 Aluminum Specimens with a Maximum Stress of 15 and a Load Ratio of 0.3 as a Function of Crack Length.....	76
A-5	Crack Growth Rate for the Back Surface of 7075-T651 Aluminum Specimens with a Maximum Stress of 15 and a Load Ratio of -0.3 as a Function of Crack Length.....	77
A-6	Crack Growth Rate for the Back Surface of 7075-T651 Aluminum Specimens with a Maximum Stress of 20 and a Load Ratio of -0.5 as a Function of Crack Length.....	78
A-7	Crack Growth Rate for the Back Surface of 7075-T651 Aluminum Specimens with a Maximum Stress of 15 and a Load Ratio of -0.5 as a Function of Crack Length.....	79
A-8	Crack Growth Rate for the Front Surface of 7075-T651 Aluminum Specimens with a Maximum Stress of 20 and a Load Ratio of 0.1 as a Function of Crack Length.....	80
A-9	Crack Growth Rate for the Front Surface of 7075-T651 Aluminum Specimens with a Maximum Stress of 15 and a Load Ratio of 0.1 as a Function of Crack Length.....	81
A-10	Crack Growth Rate for the Front Surface of 7075-T651 Aluminum Specimens with a Maximum Stress of 20 and a Load Ratio of 0.3 as a Function of Crack Length.....	82
A-11	Crack Growth Rate for the Front Surface of 7075-T651 Aluminum Specimens with a Maximum Stress of 15 and a Load Ratio of 0.3 as a Function of Crack Length.....	83
A-12	Crack Growth Rate for the Front Surface of 7075-T651 Aluminum Specimens with a Maximum Stress of 15 and a Load Ratio of -0.3 as a Function of Crack Length.....	84
A-13	Crack Growth Rate for the Front Surface of 7075-T651 Aluminum Specimens with a Maximum Stress of 20 and a Load Ratio of -0.5 as a Function of Crack Length.....	85

Figure		Page
A-14	Crack Growth Rate for the Front Surface of 7075-T651 Aluminum Specimens with a Maximum Stress of 15 and a Load Ratio of -0.5 as a Function of Crack Length.....	86

List of Tables

Table		Page
1	Initial Crack Sizes and Shapes for PMMA	15
2	Stress Ratios, Maximum Stress Levels, and Initial Crack Sizes and Shapes for 7075-T651 Aluminum	20
3	Experimental Stress Intensity Factors Along Bore	30
4	Experimental Stress Intensity Factors at Surface	32
5	Corrected Model Life Predictions	61
6	Newman-Bowie Model Life Predictions	63
7	Brussat Model Life Predictions	65
8	Final Crack Shape Predictions at Back Surface Penetration	66

AFIT/GAE/AA'83D-17

Abstract

This study developed correction factors for currently used stress intensity factor equations to more accurately predict stress intensity factors for a corner crack emanating from a hole as it transitions to a uniform through-the-thickness crack. These correction factors resulted in an approximate 15 percent increase in total life prediction and a far better correlation between analytical stress intensity factor predictions and experimental results in the transition region. The material used for total life predictions was 7075-T651 Aluminum, and the initial crack eccentricity, a/c, was always greater than one.

Correlations were accomplished between experimental results from Polymethylmethacrylate (PMMA) testing and the Newman-Raju three-dimensional stress intensity factor equation for a single corner crack at a hole where the crack eccentricity is greater than one. These correlations were plotted from crack initiation until back surface penetration for both the top surface and along the bore of the hole. From these plots correction factors were determined and a transition region starting point was located. The transition region begins when the normalized crack depth reaches 0.75.

Correlations were also accomplished between experimental results from 7075-T651 Aluminum testing and the Grandt linearization of the Bowie equation for a through-crack emanating from a hole. These

correlations were plotted from back surface penetration to final fracture. The plot yields the end of the transition region, and also the required correction factors to be utilized. The transition region ends when the normalized crack length reaches 2.5.

Life predictions were then made using the corrected model, Engle's model, (which includes the Newman-Raju equation and Grandt's linearization of the Bowie equation), and Brussat's model. The corrected model produced better predictions than the Engle model in total life, and in predicting life from back surface penetration to final fracture for constant amplitude loading. The corrected model yields a slightly more conservative crack shape and life prediction from crack initiation until back surface penetration than the Engle model.

TRANSITION OF CORNER CRACKS AT HOLES INTO

THROUGH-THE-THICKNESS CRACKS

I. Introduction

1.1 Motivation

Cracks in aerospace structures have caused catastrophic failures resulting in loss of life, destruction of millions of dollars in equipment, and have severely reduced operational capabilities. While the elimination of conditions for crack initiation and growth is a worthwhile endeavor, the fact remains that flaws due to material defects, manufacturing methods, and in-service conditions will always be present to some extent. This simple admission opens the door to design against failure in the presence of flaws existing at the onset of operational use and during periods of fatigue growth. The fact that a crack exists is, by itself, no longer a criterion for the scrapping of an aerospace system, nor is it sufficient reason for extensive modifications.

A comprehensive review of aerospace structural failures completed by the United States Air Force in 1971 (1) showed the origin of failures due to cracks, in order of decreasing frequency of occurrence, to be: (1) Cracks emanating from fastener holes; (2) Corner cracks; (3) Surface cracks. Over one-third of all failures studied were due to cracks emanating from fastener holes. The neccessity to accurately predict the life of aerospace structures through fracture analysis is clear, since

some of today's transport aircraft contain over one million fastener holes. In order to ensure that catastrophic failures of aerospace structures do not occur at these locations, the United States Air Force has recently adopted a damage tolerant design philosophy (2). This philosophy is based on the use of fracture mechanics.

The use of fracture mechanics in the analysis of flawed fastener holes requires an in-depth knowledge of the stress intensity factor, K, for the structural and crack geometries of interest. Analytical determination of these stress intensity factors is dependent on various correction factors and can become quite involved. These factors are generally derived using experimental data and backtracking, finite element approximations, or engineering judgement. These factors relate specimen geometry, loading, and crack characteristics, such as crack length. Because of their importance, several investigations have been carried out for corner cracks at fastener holes over the past several years (see e.g. 3-7). One of the areas that still needs to be addressed is the transition from a corner crack to a uniform through-the-thickness crack, since the prediction of an aerospace structure's life is heavily influenced by the large number of these regions. Several investigators (21-26) have looked at this region in recent times. These studies are summarized in the following sections.

1.2 Background

1.2.1 Stress Intensity Factors for Corner Cracks Emanating from a Hole. The first major advance in the study of cracks emanating from open holes in plates was due to Bowie (3) in 1956. He solved the two

dimensional problem of single and double through-cracks at an open hole using complex variable methods. Although not an exact solution, Bowie's results have served as the basis in the framing of other studies. Perhaps more important is the almost universal use of his solution to establish the accuracy of other methods designed to provide answers for the more complicated problems being investigated today.

Tweed and Rooke (4) considered the single through-crack problem at a later date. They used integral transform techniques to derive stress intensity factor relationships. Their solution is more accurate, especially for smaller crack lengths, than the Bowie solution.

Kobayashi (5) estimated stress intensity factors for a semi-elliptical embedded crack adjacent to an open fastener hole in a very thick plate (plane strain case). The stress intensity factor for the elliptical crack was formed by applying a shape correction to the circular crack solution. Surface effects and the through-thickness stress variation seen in the three-dimensional problem were neglected.

In 1972, Liu (6) considered a quarter-circular crack at a hole in a plate. He applied Smith's solution (7) to approximately account for the hole surface and front surface, Kobayashi's solution (8) as an approximate back surface correction, and Bowie's two-dimensional solution (3) to approximate the three-dimensional hole effect. The resulting stress intensity estimate was limited to a point on the crack periphery midway between the front and hole surfaces.

In 1974, Shah (9) completed one of the more detailed analyses. He began with the plane strain stress distribution near a hole in a plate

under uniaxial loading. He then derived expressions for stress intensity factors using a Green's function approach. Crack shape correction factors were applied to extend this estimate to elliptical cracks. Shah and Kobayashi's (10) results were applied as approximate back surface correction factors. A constant front surface correction, independent of location on the crack border, was introduced. Lastly, a factor was proposed for relating single-crack results to those for double-cracks.

In 1974, Grandt (11) applied a linear superposition technique to the Bowie solution to obtain an equation to replace the use of tables. Han and Liu (12) developed a two-dimensional solution using a back-tracking method in 1977. They used Bowie's hole correction factor (3), Isida's finite width correction factor (13), and a combined crack shape and front surface correction factor.

Newman and Raju (14) studied a wide variety of three-dimensional crack configurations subjected to uniform tension. They examined the influence of several parameters such as the parametric angle, the crack depth, the crack length, the plate thickness, and the hole radius. They curve fit three-dimensional finite element results from their previous investigations (15) to obtain equations for various correction factors. Their finite width correction factor is based on the stress concentration at the hole (16) and the crack eccentricity (17). The parametric angle factor is from Irwin's solution (18) for an embedded elliptical crack in an infinite solid. Shah's double to single crack conversion factor (9) was evaluated and found to be in good agreement with the results of Smith and Kullgren (19).

In a recent Air Force Wright Aeronautical Laboratories' Technical Memorandum, Heckel and Rudd (20) evaluated Shah's, Liu's, and Newman's stress intensity factors for corner cracks at holes. Newman and Raju's solution showed excellent results in all categories, except as the crack length along the bore of the hole approached the plate thickness.

1.2.2 Transition of a Corner Crack at a Hole to a Through-the-Thickness Crack. When the corner crack tip along the bore of the hole penetrates the back surface, the crack enters a transition stage which terminates when it becomes a uniform through-the-thickness crack. The procedures described in literature and in use today range from ignoring this transitional behavior to establishing various criteria for dealing with it. The American Society for Testing and Materials has been one of the most active proponents for the development of transition criteria. They have sponsored round-robin competitions for predicting the life of specimens to determine the accuracy of current procedures. They published a Special Technical Publication (21) in 1979 which dealt strictly with part-through crack fatigue life prediction.

Vroman and Peterson (22) developed two criteria based on back surface yielding. Their initial criterion in 1972 was shown to be more conservative than the Kobayashi-Moss (23) solution. The addition of one higher order term in 1976 provided a better approximation to the Kobayashi-Moss solution, which is very complex to program. This criterion is a function of crack depth, thickness, and crack eccentricity.

Johnson (24) tried to compensate for the overly conservative procedure of assuming a through-crack once the crack depth equals the thick-ness. He noted that once the crack penetrated the back surface it still maintained its elliptical shape until it truly became a through-crack. His criterion is based upon an imaginary crack depth, which is arrived at by allowing the flaw to continually grow in the same elliptical shape it had when it penetrated the back surface. Using his imaginary crack shape equation, the back surface crack length can be determined. When the back surface crack length is 90% of the front surface crack length, transition has ended and the crack can be considered a through-crack. This technique is mathematically simple, logical, and in good agreement with actual trends of experimental data.

Brussat and Chiu (25) predicted that during the transition region the surface flaw was neither a surface flaw nor a through crack but was actually a combination of both. They developed a criterion based upon crack depth, crack length and plate thickness for a quarter circular corner flaw at a hole. Their correction factor is a product of engineering judgement rather than mathematics.

The most commonly used procedure was referenced by Engle (26). In this procedure Newman and Raju's corner crack solution is used until the crack depth is equal to the plate thickness; then the crack length on the surface at that point is assumed to be a through-crack which follows Grandt's curve fit solution (11) to Bowie's solution (3) for a through-crack near a hole. This procedure has been adopted as the current damage tolerance philosophy of the United States Air Force. Since it

does not consider the region from back surface penetration to a through-crack, it is a conservative approach to life prediction.

1.3 Problem Statement

To accurately predict stress intensity factors for a corner crack emanating from a hole as it transitions to a uniform through-the-thickness crack (Fig 1). For the part-elliptical corner crack, the crack center is located at the intersection of the hole wall and the front surface, and the crack lies in a plane perpendicular to the axis of loading. The finite plate geometry and loading conditions are such that the plane of the crack is a plane of symmetry for the open hole problem. The loading is a remote uniaxial constant amplitude loading, and the initial crack eccentricity, a/c, is greater than one.

1.4 Objectives

The objectives of this thesis are to:

1. Evaluate the ability of existing stress intensity factor models to predict the behavior of a corner crack at a hole as it transitions to a uniform through-the-thickness crack.
2. Calculate correction factors for existing models to be applied when the predictions become unconservative beyond the confidence limit.
3. Accurately define the point where the corner crack begins its transition to a uniform through-the-thickness crack

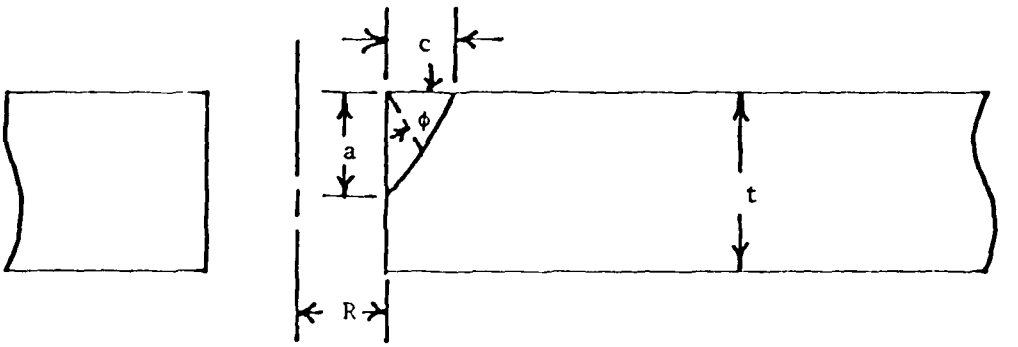

1a. Corner Crack Configuration

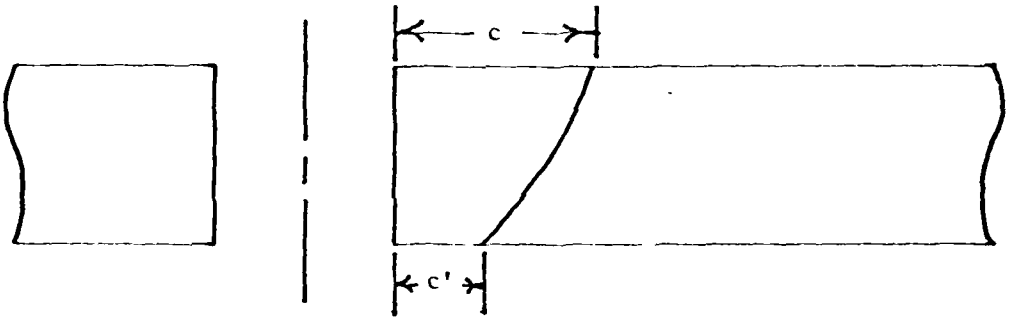

1b. Crack Configuration after Back Surface Penetration

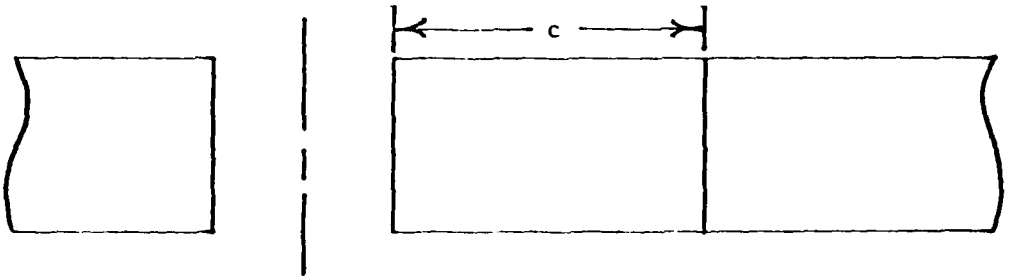

1c. Crack Configuration as a Through-the-Thickness Crack

Figure 1: Crack Configurations as it Transitions from a Corner Crack to a Through-the-Thickness Crack

and where the transition has been completed.

4. Assess the accuracy of the corrected models by comparing the total life prediction obtained using these models to results of other investigations.

1.5 Approach

Using the results of Heckel and Rudd's report (20), Newman and Raju's (14) three-dimensional stress intensity factor equation was used as the analytical solution for a single quarter-elliptical corner crack at a hole where the initial crack eccentricity is greater than one. This equation was used until the crack penetrated the back surface. These results were then compared to the experimental values found by Heckel and Rudd. The results were nomalized by dividing the analytical stress intensity factor by the experimental value. These normalized results were then plotted as a function of the normalized crack depth, that is the crack depth divided by the plate thickness. From this plot the non-dimensional transition region starting point was found. The inverse of a polynomial curve fit for the normalized stress intensity factors from the starting point of the transition region to the back surface was used as the correction factor. This procedure was accomplished along both the bore of the hole and the top surface.

Corner crack experiments were carried out by Heckel and Rudd (29) on 7075-T651 Aluminum using constant amplitude loading with varying stress ratios, R. The crack size was measured with microscopes during the test on both front and back surfaces. From this data the crack

growth rate was found. Using the James-Anderson backtracking technique and the values for Walker's equation found from baseline crack growth rate data, the experimental stress intensity factors were then computed for the corner cracks. Grandt's curve fit solution for Bowie's equation was the analytical solution used after back surface penetration took place. The normalized stress intensity factors were computed as before and plotted for both the front and back surfaces. The normalized crack lengths, the respective crack lengths divided by the radius of the hole, were used as the independent variable. The inverse of a polynomial curve fit for the data on each surface was used as the correction factor for the corresponding surface. A relationship between the normalized crack lengths on the front and back surfaces was also developed. This relationship allows the stress intensity factor corrections to be computed on both surfaces knowing only the front surface crack length and hole radius.

The superposition of the stress intensity factor models with their appropriate corrections was then used to predict total fatigue lives for seven 7075-T651 Aluminum specimens. The results from these predictions were then compared to the actual lives and life predictions which used different models, along with crack shape prediction comparisons.

II. Testing

2.1 Polymethylmethacrylate (PMMA) Testing

2.1.1 Crack Growth Rate Tests. The basic crack growth rate tests for PMMA were conducted by Grandt and Hinnerichs (27). The tests were conducted for the compact tension, 3-point bend, and 4-point bend specimens schematically illustrated in Figure 2. Details of these tests are documented in Reference 27.

The crack growth rate data from these tests were then curve fitted to the Paris equation. The best-fit Paris equation was found to be:

$$da/dN = 6.94918 \times 10^{-23} \quad (\Delta K)^{6.095445} \qquad (1)$$

where ΔK is the stress intensity factor range defined as $K_{MAX}-K_{MIN}$. The units of da/dN and ΔK in equation 1 are inch/cycle and psi x $in^{1/2}$, respectively. For a given da/dN value, the upper and lower bounds for the data are the mean value (Eqn 1) plus or minus 17%, respectively. These bounds account for the total amount of scatter for the test data due to experimental error, human error in making the crack growth readings, material property variations, etc.

2.1.2 Corner-Crack-at-a-Hole Tests. Tests of PMMA specimens were conducted for a single corner crack at a hole. These tests were conducted by Grandt and Snow (28). The specimen geometry is shown in Figure 3. These specimens were made from 8 inches by 14 inches by .72 inch bulk PMMA plate. The hole diameter was .75 inch. The specimens were pre-cracked at a maximum stress of 780 psi. After a crack

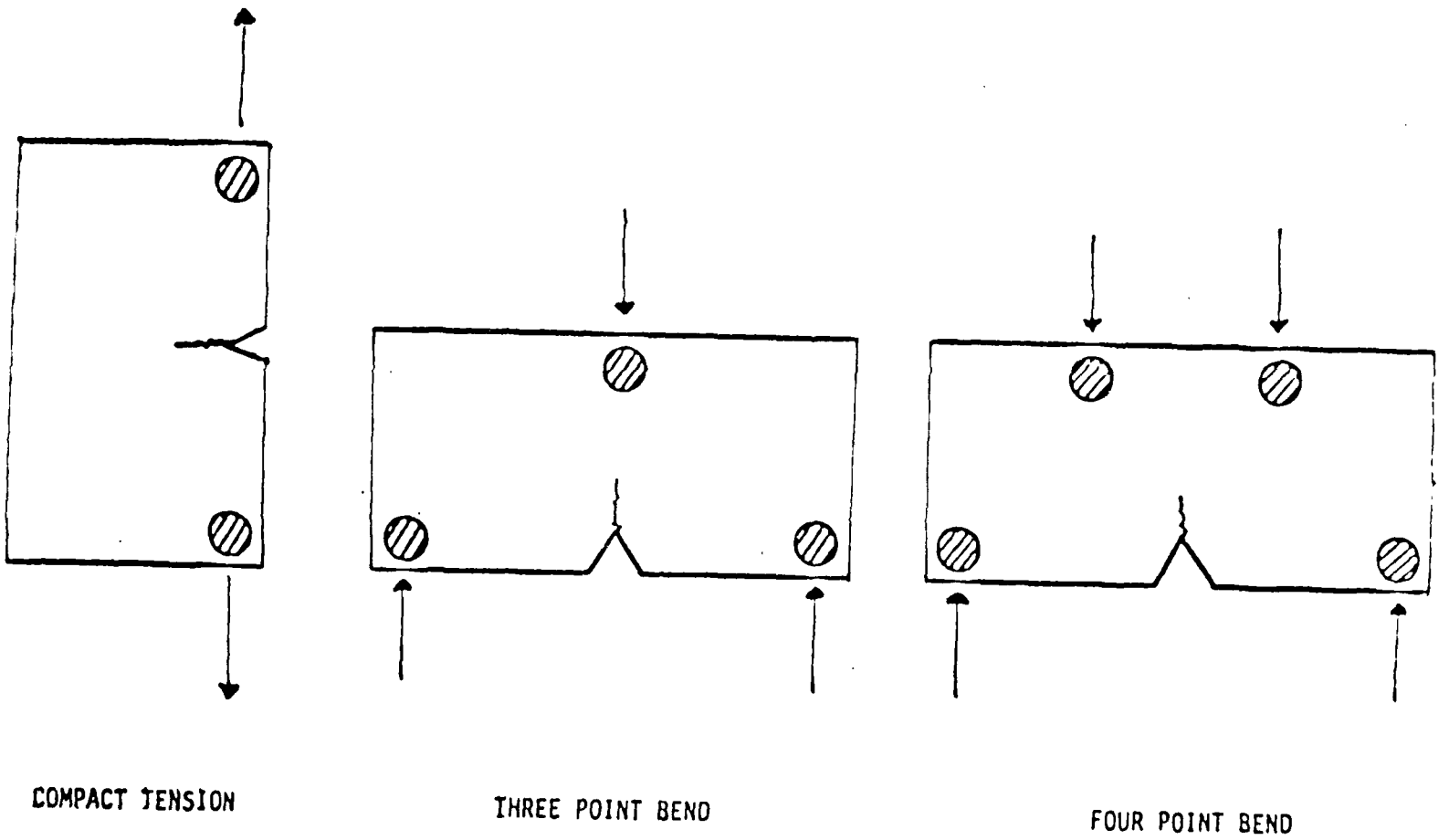

Figure 2: Schematic of Tests Conducted by Grandt and Hinnerichs

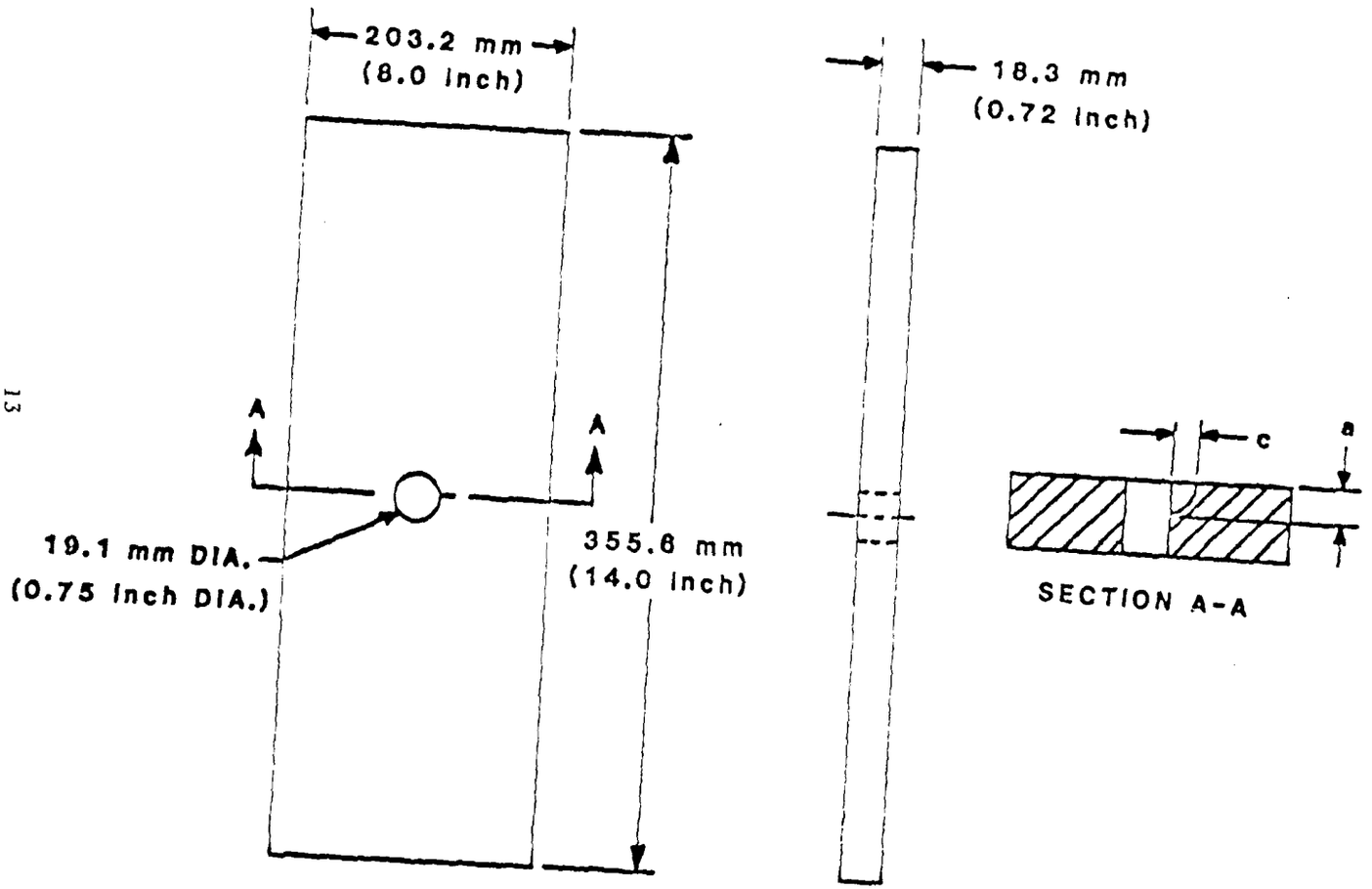

Figure 3: Specimen Geometry Used by Grandt and Snow

initiated, the crack growth tests were conducted at a maximum stress of 590 psi and a stress ratio of .029. The initial crack lengths and shapes for the five specimens considered in this study are presented in Table 1.

Although seven corner-crack-at-a-hole tests were conducted in Reference 28, only five are considered in this study. Two tests were omitted due to insufficient data and excessive pinning, that is restricting of the crack growth, at the front surface. Justification for omitting these two tests is given in Reference 20. Minor pinning still occured on the front surfaces of the five test specimens considered in this study. It could be caused by free surface effects, residual stresses, or a number of other reasons. The minor pinning prevented the maximum crack dimension measured from the bore of the hole from occurring at the front surface. The test results indicated that the maximum crack dimension measured from the hole wall occurred at approximately 10° from the front surface. Because the Newman and Raju solution (14) assumes an elliptical crack shape, the predicted maximum crack dimension from the bore of the hole would occur at the front surface. The analytical stress intensity factor should not be expected to predict the pinning action, particularly if residual stresses were present. Therefore the experimental crack shape was extrapolated from the maximum crack dimension measured from the bore of the hole to the free surface using an elliptical equation. These extrapolated crack lengths were used in the comparisons with the predicted surface crack lengths. The extrapolated final crack lengths for the five cases considered were 3 to 18 percent longer than those measured during the tests.

TABLE 1 - INITIAL CRACK SIZES AND SHAPES FOR PMMA

TEST NO.	a_I, mm (INCH)	c_I, mm (INCH)	$(a/c)_I$
1	5.77 (.227)	3.66 (.144)	1.58
3	4.11 (.162)	4.29 (.169)	0.96
5	4.27 (.168)	3.43 (.135)	1.25
6	3.05 (.120)	2.69 (.106)	1.13
8	4.24 (.167)	3.23 (.127)	1.31

Since PMMA is a transparent material, 35 mm camera pictures could be taken during the tests to provide a record of the flaw shape changes. This procedure allowed growth intervals as small as .005 inch to be measured. Measurements were not taken once back surface penetration occurred.

2.2 7075-T651 Aluminum Testing

2.2.1 Crack Growth Rate Tests. Crack growth rate tests for 7075-T651 Aluminum were conducted at the Air Force Wright Aeronautical Laboratories (29). Duplicate specimens were tested for each test condition in a laboratory air environment. The temperature and relative humidity ranges were 68° to 72° F and 50% to 65%, respectively. The test specimens were subjected to a one Hertz loading frequency. The tests were conducted for stress ratios of 0.1, 0.5, and -0.5. The geometry of the center-crack-tension specimens tested is shown in Figure 4.

The crack growth rate data for the positive stress ratio tests for the 7075-T651 Aluminum specimens were then curve fit to Walker's equation using Grimsley's procedure (30). The best fit Walker's equation to the data was found to be:

$$da/dN = 3.2624 \times 10^{-9} \left[(1-R)^{-\frac{1}{2}} \Delta K\right]^{3.3908} \qquad (2)$$

where the units of da/dN and ΔK in Equation 2 are inch/cycle and ksi x $inch^{\frac{1}{2}}$, respectively. For a given da/dN value, the upper and lower bounds containing 97.7% of the data are the mean value plus or minus 12% respectively. These bounds account for almost all the scatter in the

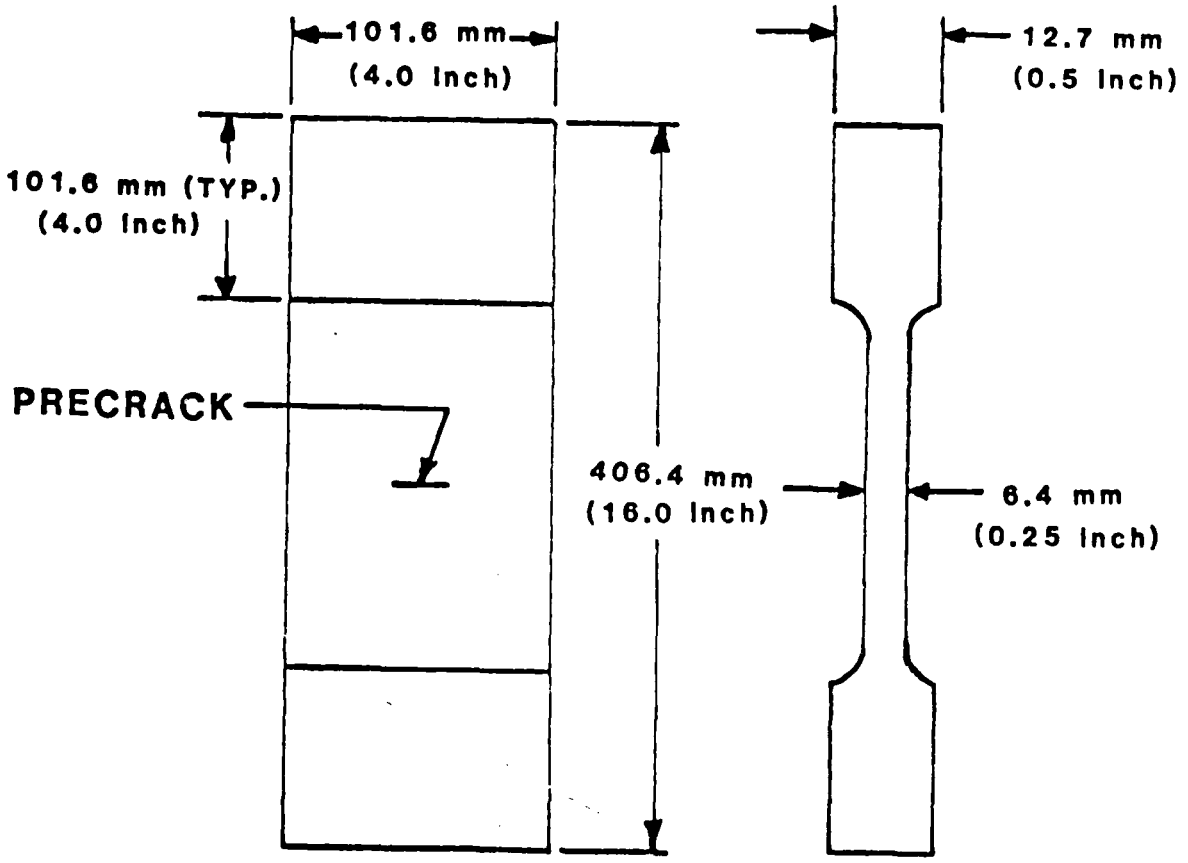

Figure 4: Center-Crack-Tension Specimen Geometry Used by Heckel and Rudd

test data due to experimental error, human error, material property variations, etc.

The crack growth rate for the negative stress ratio tests for the 7075-T651 Aluminum specimens was then curve fit to Walker's equation as discussed earlier. The best-fit Walker's equation was found to be:

$$da/dN = 1.29 \times 10^{-8} \left[\Delta K/(1-R) \right]^{2.89} \qquad (3)$$

where the units of da/dN and ΔK are the same as in Equation 2. The data for the negative stress ratio tests had the same error as the positive ratio tests, plus or minus 12%.

2.2.2 Corner-Crack-at-a-Hole Tests. Tests of 7075-T651 Aluminum were conducted for a single corner crack at a hole. These tests were performed at the Air Force Wright Aeronautical Laboratories. The specimen geometry is shown in Figure 5. The specimens were precracked at the same constant amplitude stress levels used in the crack growth rate tests. The maximum stress levels used for testing after precracking were 20 ksi and 15 ksi. Two positive stress ratios (0.1 and 0.3) and two negative stress ratios (-0.3 and -0.5) were considered. The maximum stress level, stress ratio, and initial crack size and shape are presented in Table 2 for the seven test conditions considered. Duplicate tests were run for each loading condition and averaged in order to eliminate bias due to a single faulty test at one or more load conditions.

Crack length measurements along the bore of the hole could not be made for the 7075-T651 Aluminum specimens during the test since these

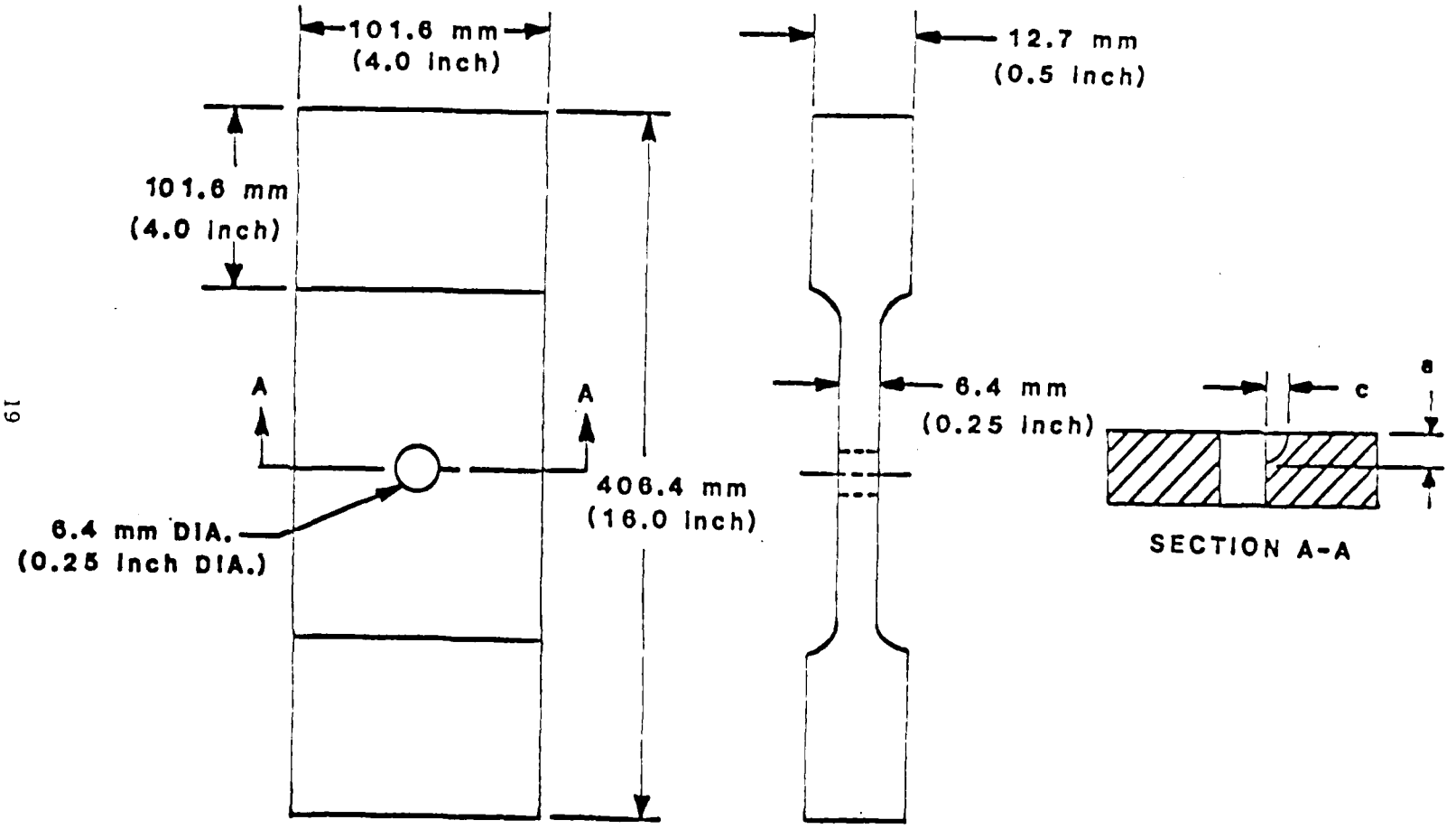

Figure 5: Specimen Geometry Used for 7075-T651 Aluminum Testing

TABLE 2 - STRESS RATIOS, MAXIMUM STRESS LEVELS, AND INITIAL CRACK SIZES AND SHAPES FOR 7075-T651 AL

SPECIMEN NO.	R	σ_{MAX}, MPa (KSI)	a_i, mm (INCH)	c_i, mm (INCH)	$(a/c)_i$
FH-7	0.1	137.9 (20.0)	1.88 (.074)	1.35 (.053)	1.40
FH-10	0.1	103.4 (15.0)	2.26 (.089)	1.27 (.050)	1.78
FH-8	0.3	137.9 (20.0)	1.93 (.076)	1.30 (.051)	1.49
FH-11	0.3	103.4 (15.0)	2.59 (.102)	1.27 (.050)	2.04
FH-13	-0.3	103.4 (15.0)	2.46 (.097)	1.35 (.053)	1.83
FH-9	-0.5	137.9 (20.0)	1.80 (.071)	1.27 (.050)	1.42
FH-12	-0.5	103.4 (15.0)	2.06 (.081)	1.30 (.051)	1.59

specimens are not transparent. In order to obtain a limited number of crack length measurements along the bore of the hole after the tests were completed, marker loads were applied during the test. These marker loads consisted of the same maximum constant amplitude stress levels used in the tests, but the minimum stress levels were increased so that the stress ratio was 0.85. The marker loads produced striations on the fracture surfaces which were measured with an optical microscope after the completion of the tests. The marker loads were applied at surface crack lengths of .05 in, .08 in, .12 in, and .16 in. The crack growth rates due to the constant amplitude loading were determined both before and after each set of marker loads was applied. From this, an average constant amplitude crack growth rate was determined for each associated marker band. The width of each marker band was divided by the associated average constant amplitude crack growth rate to obtain the number of constant amplitude load cycles required to produce the same amount of growth as the marker load. The number of marker load cycles for each marker band was replaced by the corresponding number of constant amplitude load cycles. Hence, this provided a method of accounting for the crack growth caused by the application of the marker loads in the experimental results.

Also, since the aluminum specimens are not transparent, the maximum crack lengths measured from the bore of the hole could not be determined during the tests. Therefore, the amount of pinning, (restriction of crack growth) at the free surface could not be determined for these specimens. The experimental surface crack lengths were the actual measured values on the surface, unlike the extrapolated results in

Grandt and Snow's study (28). As mentioned earlier this could result in errors up to 18 percent.

2.2.3 Corner-Crack to Final Fracture Tests. The corner-crack-at-a-hole tests for the 7075-T651 specimens were continued until failure occurred. Crack length measurements on both the front and back surfaces were taken at random intervals during the tests. The method chosen for taking these measurements used two optical microscopes mounted on the experimental apparatus, one on the front surface and the other on the back. By taking these crack length measurements and knowing the number of cycles between each measurement the resulting crack growth rates for both surfaces were computed.

III. Experimental Stress Intensity Factors

3.1 Corner-Crack-at-a-Hole until Back Surface Penetration

Experimental stress intensity factors were determined for the corner-crack-at-a-hole tests for the PMMA material, but not for the 7075-T651 Aluminum specimens. This was possible for the PMMA material because large amounts of crack growth data were recorded during the tests, both on the front surface and along the hole wall. However, this was not possible for the aluminum specimens.

The experimental stress intensity factors were obtained using the James-Anderson backtracking technique (31). The technique is illustrated in Figure 6 and is described as follows:

1. Crack growth curves were determined from the corner-crack-at-a-hole tests previously described. The curves were determined at the wall of the hole (a vs. N) and at the front surface (c vs. N).
2. Crack growth rates were determined from the crack growth curves for the corner cracks. A standard seven point polynomial method, recommended by ASTM, was used to determine the crack growth rates. The crack growth rates were expressed as functions of the crack length (da/dN vs. a and dc/dN vs. c).
3. For a given crack length and corresponding crack growth rate, the associated stress intensity factor was calculated from the Paris equation (see Eqn 1) as

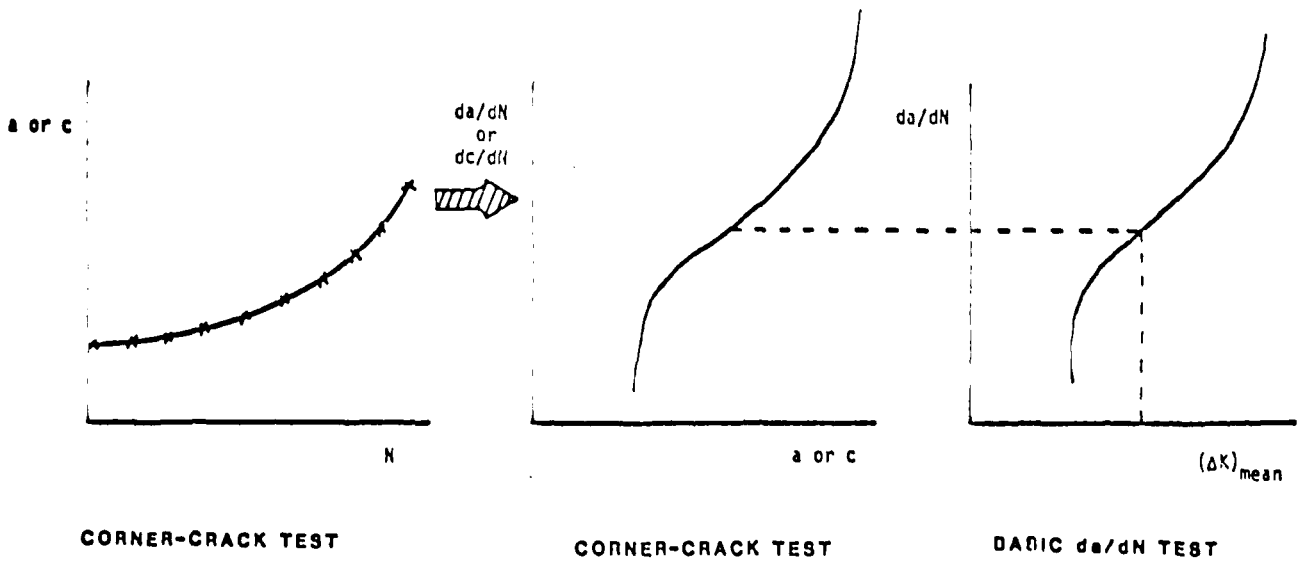

Figure 6: Schematic of James-Anderson Backtracking Technique

$$\Delta K = [da/dN \ / \ (6.94918 \times 10^{-23})]^{1/6.095445} \qquad (4)$$

where ΔK is the mean stress intensity factor. This result is the experimental stress intensity factor along the bore of the hole. For the experimental stress intensity factor along the surface, dc/dN should be substituted for da/dN.

3.2 Back Surface Penetration Until Final Fracture

Experimental stress intensity factors were determined from back surface penetration to final fracture tests for the 7075-T651 Aluminum specimens but not for the PMMA material. This was possible for the aluminum specimens because large amounts of crack growth data were recorded during the tests for both the front and back surfaces. However this was not accomplished for the PMMA specimens.

The experimental stress intensity factors were obtained using the James-Anderson backtracking procedure, outlined in the preceding section, with the following changes:

1. The crack growth curves were determined at the back surface (c' vs. N) and the front surface (c vs. N).
2. The crack growth rates were expressed as a function of crack length (dc'/dN vs. c' and dc/dN vs. c). The crack growth rate was then curve-fit using a polynomial regression technique. This polynomial curve fit allows the crack growth rate to be calculated at any crack length. These curve fits are shown in the Appendix.

3. The associated stress intensity factor for positive stress ratios was found using the Walker's equation (see Eqn 2) as

$$\Delta K = [dc/dN \ / \ (3.2624 \times 10^{-9})]^{1/3.3908} \ (1 - R)^{1/2} \qquad (5)$$

for the front surface. For the back surface, dc'/dN should be substituted for dc/dN.

The associated stress intensity factor for negative stress ratios was found from Walker's equation (see Eqn 3) as

$$\Delta K = [dc/dN \ / \ (1.29 \times 10^{-8})]^{1/2.89} \ (1 - R) \qquad (6)$$

for the front surface. For the back surface, the substitution as described before should be used.

IV. Analytical Stress Intensity Factors

4.1 Analytical Solution Used for the Corner Crack

Using the results of Heckel and Rudd's studies (20, 29), Newman and Raju's three-dimensional finite-element solution (14) was chosen as the analytical solution to be used in this study. This solution was chosen because of its accuracy as outlined by Heckel and Rudd (20, 29). The Newman-Raju solution is one of the most commonly used solutions in aerospace industry today.

The Newman equation used was for an initial a/c, which is crack depth divided by crack length, greater than one (14). The problem is schematically shown in Figure 1a. The resulting equation used is:

$$\Delta K_I = \Delta S \sqrt{\pi a/Q} \; F_{CH}(a/c, a/t, R/t, c/b, \phi) \; F_{SH} \tag{7}$$

where

$$\Delta S = S_{MAX} (1 - R) \tag{8}$$

$$Q = 1 + 1.464(c/a)^{1.65} \tag{9}$$

$$F_{CH} = [M_1 + M_2(a/t)^2 + M_3(a/t)^4] \; g_1 \; g_2 \; g_3 \; f_\phi \; f_w \tag{10}$$

$$M_1 = \sqrt{c/a} \; (1 + 0.04(c/a)) \tag{11}$$

$$M_2 = 0.2 \; (c/a)^4 \tag{12}$$

$$M_3 = -0.11 \; (c/a)^4 \tag{13}$$

$$g_1 = 1 + [0.1 + 0.35(c/a)(a/t)^2] \; (1 - \sin\phi)^2 \tag{14}$$

$$g_2 = [1 - 0.15\lambda + 3.46\lambda^2 - 4.47\lambda^3 + 3.52\lambda^4]/[1 + 0.13\lambda^2] \tag{15}$$

$$\lambda = [1 + (c/R) \cos(0.85\phi)]^{-1} \tag{16}$$

$$g_3 = [1.13 - 0.09(c/a)][1 + 0.1(1 - \cos\phi)^2][0.8 + 0.2(a/t)^{1/4}] \tag{17}$$

$$f_\phi = [(c/a)^2 \sin^2\phi + \cos^2\phi]^{1/4} \tag{18}$$

$$f_w = [\sec(\pi R/2b) \sec(\sqrt{a/t}\,(\pi(2R + c))/(4(b - c) + 2c))]^{1/2} \tag{19}$$

$$F_{SH} = [(4/\pi + ac/2tR) \;/\; (4/\pi + ac/tR)]^{1/2} \tag{20}$$

The details of this solution are given in Reference 14 and will not be discussed here.

4.2 Analytical Solution Used for the Through-Crack

Grandt's curve fit solution to the Bowie equation presented by Engle in Reference 26 was chosen as the analytical solution to be used after back surface penetration has occurred. The equation, given in Reference 26, is

$$\Delta K_I = \Delta S \sqrt{\pi c}\, F_{GR}(c/R)\, f_w \tag{21}$$

where

$$F_{GR} = .6762062 + [.8733015/(.3245442 + c/R)] \tag{22}$$

and ΔS and f_w are as given in equations 8 and 19, respectively. The details for this solution are discussed in Reference 26 and will not be repeated here.

V. Analytical/Experimental Correlations

5.1 Corner Crack Until Back Surface Penetration

Correlations were made of the experimental stress intensity factor ranges with the analytical predictions for the PMMA material for the corner crack until back surface penetration region. The experimental stress intensity factor ranges obtained using the James-Anderson backtracking technique (28) were based on mean crack growth rate data. This correlation was accomplished by dividing the analytical stress intensity factor ranges by the experimental values at specific points, both along the bore of the hole and the front surface. The points chosen were the ones presented by Heckel and Rudd (20), and they are listed in Tables 3 and 4. The independent variable that was chosen was the normalized crack depth (a/t), since this variable appears to have more influence than the crack eccentricity (a/c) has.

The correlations along the bore of the hole are plotted in Figures 7 and 8. In these figures an ideal correlation would yield all values equal to one. It can be seen that the values are conservative, that is the values are greater than one, until approximately one-half of the way through the material where they become unconservative. There appears to be a step where the normalized crack depth is approximately equal to 0.75. This value of the normalized crack depth will be used as the start of the transition region.

The correlations along the surface of the material as a function of normalized crack depth are plotted on Figures 9 and 10. Again, on these

TABLE 3: EXPERIMENTAL STRESS INTENSITY FACTORS ALONG BORE

a (incn)	c (inch)	a/c	da/dN (inch/cycle)	ΔK_A psixin$^{1/2}$
TEST NO. 1				
0.278	0.168	1.655	1.7425E-05	715.26
0.293	0.181	1.619	2.0769E-05	736.16
0.312	0.193	1.617	2.3862E-05	753.12
0.329	0.202	1.629	2.5372E-05	760.76
0.344	0.208	1.654	2.8738E-05	776.45
0.362	0.218	1.661	3.1128E-05	786.69
0.380	0.236	1.610	3.5051E-05	802.16
0.420	0.252	1.667	3.5724E-05	804.67
0.440	0.262	1.679	3.5856E-05	805.15
0.456	0.275	1.658	3.7902E-05	812.52
0.472	0.286	1.650	4.1285E-05	824.00
0.488	0.296	1.649	4.6789E-05	841.09
0.510	0.306	1.667	5.7800E-05	870.76
0.534	0.322	1.658	6.3598E-05	884.53
0.559	0.336	1.664	6.7152E-05	892.45
0.585	0.342	1.711	7.0287E-05	899.16
0.603	0.356	1.677	7.4494E-05	907.77
0.632	0.378	1.672	9.1223E-05	938.45
TEST NO. 3				
0.245	0.208	1.178	2.2388E-05	745.28
0.261	0.219	1.192	2.4063E-05	754.16
0.290	0.222	1.306	2.5929E-05	763.46
0.318	0.238	1.336	2.8186E-05	773.98
0.347	0.258	1.345	3.2308E-05	791.51
0.376	0.276	1.362	3.7038E-05	809.45
0.385	0.285	1.351	4.2761E-05	828.76
0.422	0.301	1.402	4.9779E-05	849.68
0.441	0.304	1.451	5.0977E-05	853.00
0.474	0.321	1.477	5.4179E-05	861.57
TEST NO. 5				
0.226	0.176	1.284	1.2287E-05	675.42
0.252	0.189	1.333	1.5840E-[illegible]	704.16
0.279	0.214	1.304	2.1984E-05	743.06
0.305	0.227	1.344	2.6188E-05	764.70
0.336	0.238	1.412	3.2009E-05	790.30
0.368	0.261	1.410	4.1000E-05	823.06
0.404	0.278	1.453	5.0755E-05	852.39
0.458	0.292	1.568	6.2588E-05	882.21
0.537	0.321	1.673	8.0677E-05	919.73
0.573	0.336	1.705	8.8963E-05	934.60
0.589	0.347	1.697	9.0149E-05	936.63

TABLE 3: EXPERIMENTAL STRESS INTENSITY FACTORS ALONG BORE (CONT)

a (inch)	c (inch)	a/c	da/dN (inch/cycle)	ΔK_A psixin$^{1/2}$
TEST NO. 6				
0.198	0.140	1.414	1.3343E-05	684.62
0.227	0.156	1.455	1.5615E-05	702.51
0.244	0.161	1.516	1.7727E-05	717.28
0.262	0.171	1.532	2.0199E-05	732.81
0.279	0.183	1.525	2.3429E-05	750.86
0.306	0.193	1.585	2.8929E-05	777.29
0.324	0.202	1.604	3.3393E-05	795.81
0.371	0.222	1.671	3.8709E-05	815.33
0.423	0.241	1.755	4.5839E-05	838.26
0.456	0.262	1.740	5.3918E-05	860.89
0.485	0.280	1.732	5.8789E-05	873.19
0.525	0.295	1.780	6.7342E-05	892.86
0.543	0.303	1.792	7.4357E-05	907.50
0.560	0.315	1.778	7.8898E-05	916.36
0.585	0.329	1.778	8.6491E-05	930.29
0.610	0.338	1.805	1.2982E-04	994.38
0.642	0.356	1.803	2.2613E-04	1089.16
0.670	0.372	1.801	2.9867E-04	1140.03
TEST NO. 8				
0.238	0.149	1.597	1.0973E-05	663.00
0.270	0.176	1.534	1.3987E-05	689.93
0.293	0.192	1.526	1.7358E-05	714.81
0.319	0.203	1.571	1.9820E-05	730.54
0.338	0.212	1.594	2.1320E-05	739.33
0.361	0.224	1.612	2.4250E-05	755.12
0.386	0.239	1.615	2.8081E-05	773.51
0.403	0.250	1.612	3.4036E-05	798.30
0.444	0.268	1.657	4.3064E-05	829.72
0.475	0.281	1.690	4.7746E-05	843.89
0.495	0.292	1.695	5.3489E-05	859.76
0.524	0.302	1.735	5.6995E-05	868.76
0.552	0.315	1.752	6.4125E-05	885.72
0.575	0.322	1.786	7.0024E-05	898.60
0.600	0.333	1.802	7.5996E-05	910.75
0.628	0.343	1.831	7.8788E-05	916.16
0.648	0.346	1.873	7.8326E-05	915.27

TABLE 4: EXPERIMENTAL STRESS INTENSITY FACTORS AT SURFACE

a (inch)	c (inch)	a/c	dc/dN (inch/cycle)	ΔK_c psixin$^{1/2}$
TEST NO. 1				
0.329	0.202	1.629	1.5070E-05	698.43
0.362	0.225	1.609	1.7140E-05	713.33
0.399	0.247	1.615	1.9979E-05	731.49
0.440	0.262	1.679	2.1717E-05	741.57
0.463	0.277	1.671	2.4137E-05	754.54
0.483	0.292	1.654	2.6566E-05	766.50
0.520	0.312	1.667	3.2103E-05	790.68
0.545	0.328	1.662	3.6119E-05	806.12
0.592	0.346	1.711	4.3418E-05	830.83
0.614	0.368	1.668	5.1952E-05	855.66
0.652	0.388	1.680	7.8496E-05	915.60
TEST NO 3				
0.318	0.238	1.336	1.5527E-05	701.86
0.347	0.258	1.345	1.8104E-05	719.76
0.376	0.276	1.362	2.0900E-05	736.92
0.422	0.301	1.402	2.4541E-05	756.60
TEST NO. 5				
0.258	0.200	1.290	1.1910E-05	671.98
0.305	0.227	1.344	1.4782E-05	696.22
0.368	0.261	1.410	1.8294E-05	721.00
0.404	0.278	1.453	2.0854E-05	736.66
0.537	0.321	1.673	2.7393E-05	770.37
0.573	0.336	1.705	3.3882E-05	797.71
0.600	0.355	1.690	4.0542E-05	821.54
TEST NO. 6				
0.262	0.171	1.532	1.0572E-05	658.97
0.306	0.193	1.585	1.3525E-05	686.14
0.371	0.222	1.671	1.8075E-05	719.57
0.423	0.241	1.755	2.2121E-05	743.82
0.456	0.262	1.740	2.7070E-05	768.87
0.485	0.280	1.732	3.1027E-05	786.27
0.525	0.295	1.780	3.4844E-05	801.38
0.560	0.315	1.778	4.1644E-05	825.17
0.610	0.338	1.805	5.2438E-05	856.96

TABLE 4: EXPERIMENTAL STRESS INTENSITY FACTORS AT SURFACE (CONT)

a (inch)	c (inch)	a/c	dc/dN (inch/cycle)	ΔK_c psixin$^{1/2}$
TEST NO. 8				
0.283	0.183	1.546	8.7612E-06	638.96
0.319	0.203	1.571	1.0657E-05	659.83
0.361	0.224	1.612	1.3370E-05	684.85
0.386	0.239	1.615	1.5191E-05	699.34
0.444	0.268	1.657	1.9310E-05	727.42
0.495	0.292	1.695	2.2406E-05	745.38
0.552	0.315	1.752	2.7261E-05	769.76

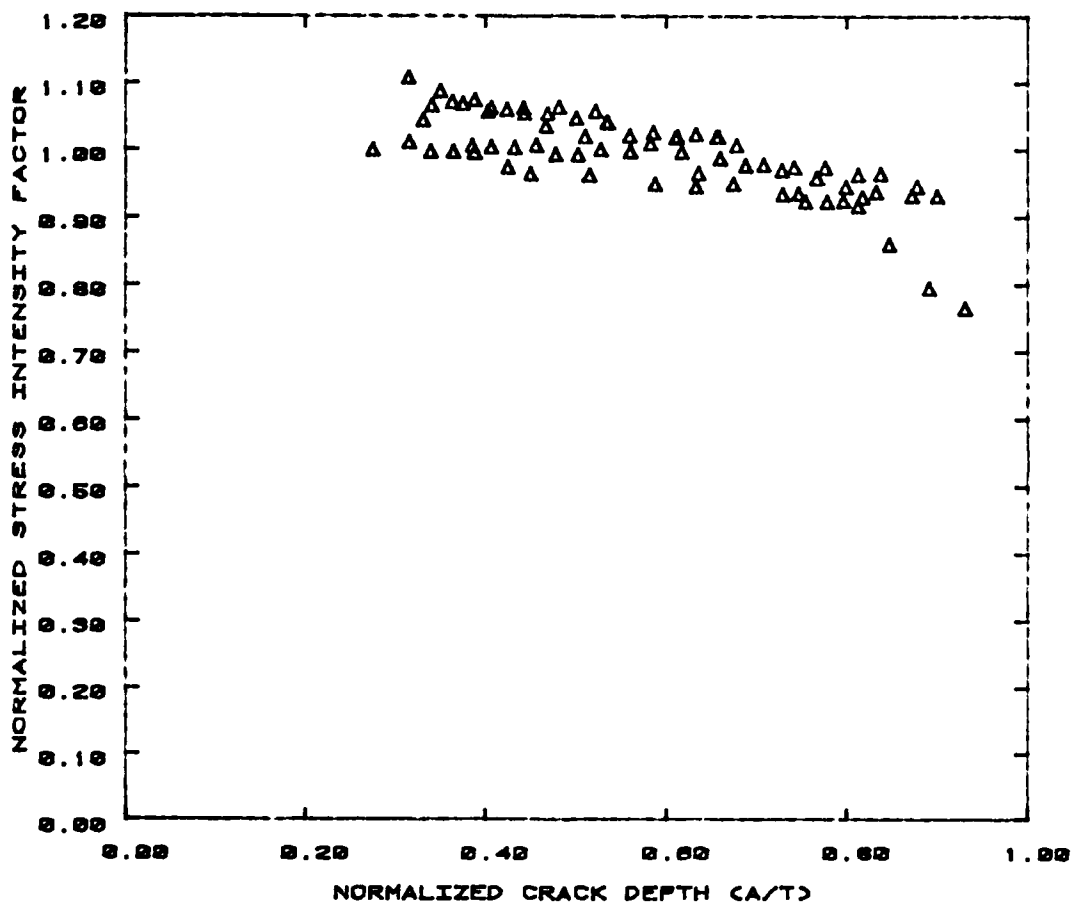

Figure 7: Correlation of Stress Intensity Factors along the Bore of the Hole for PMMA Tests

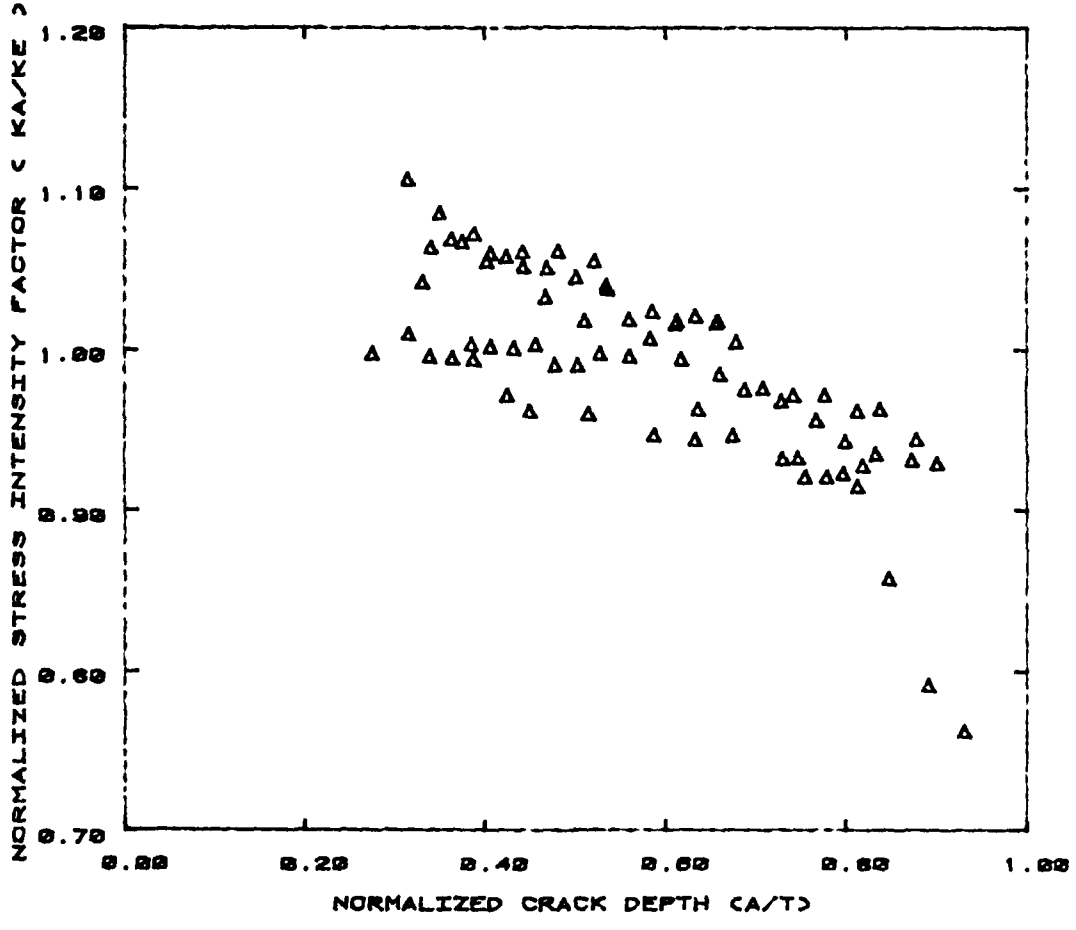

Figure 8: Correlation of Stress Intensity Factors Along the Bore of the Hole for PMMA Tests (Expanded y-axis)

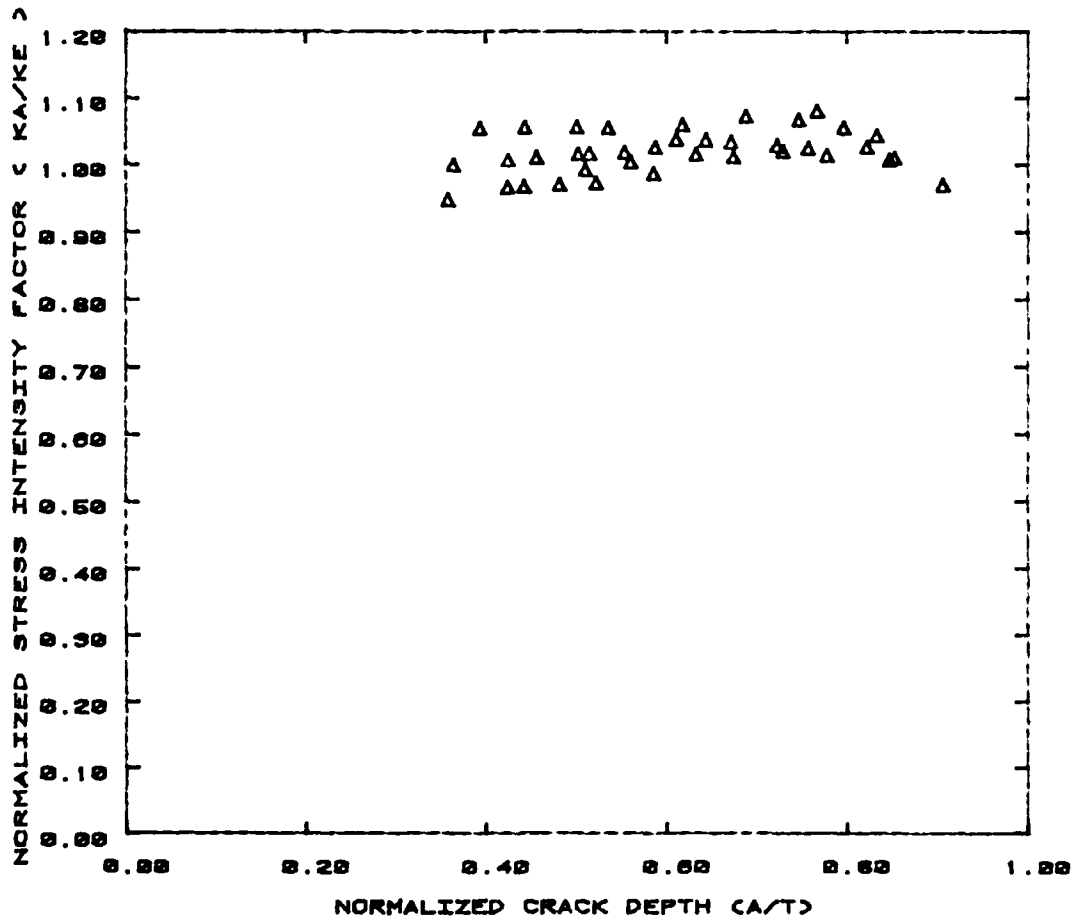

Figure 9: Correlation of Stress Intensity Factors Along the Front Surface of the PMMA Tests

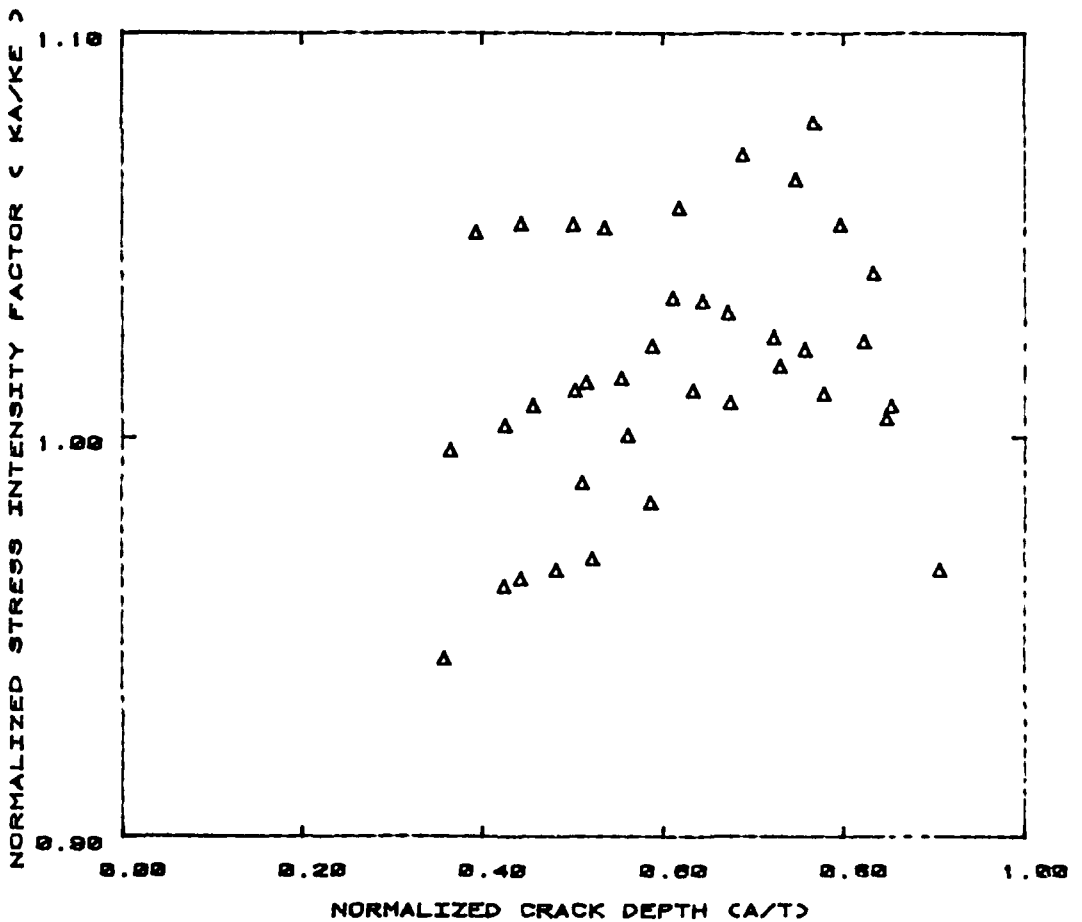

Figure 10: Correlation of Stress Intensity Factors Along the Front Surface of the PMMA Tests (Expanded y-axis)

figures an ideal correlation would be one. The correlation for this region is very good, but on Figure 9 a definite pattern is noticeable. The correlations improve until the normalized crack depth is approximately 0.75, and then they deteriorate rapidly. This value of 0.75 agrees with the value selected as the start of the transition region along the bore of the hole.

5.2 Back Surface Penetration Until Final Fracture

Correlations were made of the experimental stress intensity factor ranges with the analytical predictions for the 7075-T651 Aluminum specimens for the back surface penetration until final fracture region. Experimental stress intensity factors obtained by using the James-Anderson backtracking technique were based on mean crack growth rate data. These correlations were obtained by following the same technique as outlined in the preceding section, but rather than choosing specific points the procedure outlined in the Appendix was used. The independent variables in this region were chosen to be the normalized crack lengths (c/R and c'/R), since the crack is being treated as a through-the-thickness crack in this region.

Correlations along the back surface are plotted in Figure 11. As the value of the normalized crack length approaches 2.5, the ratio approaches unity. The value of 2.5 also coincides with the value where the back surface crack length, c', is 90 percent of the front surface crack length, c, which Johnson (24) defined as the end of the transition region in his criterion.

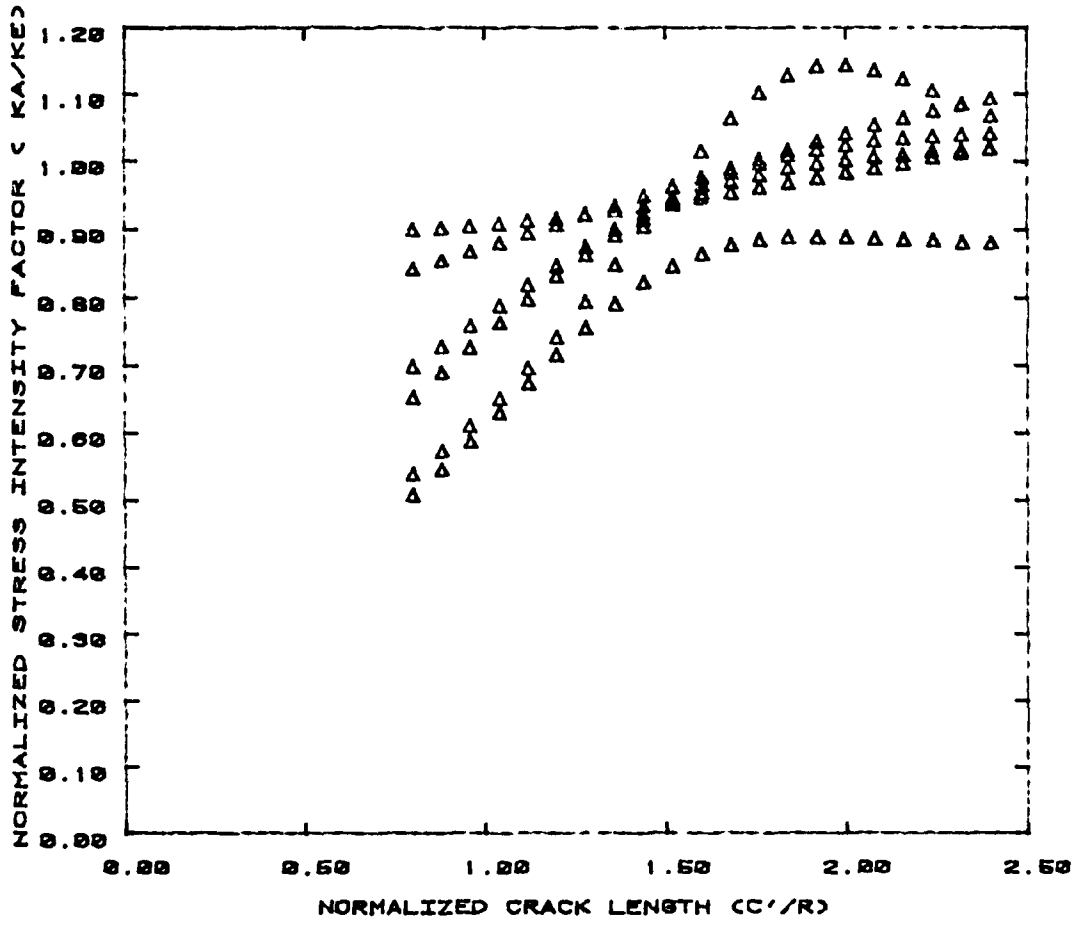

Figure 11: Correlation of Stress Intensity Factors Along the Back Surface of the 7075-T651 Aluminum Tests Until Normalized Crack Length Equals 2.5

Correlations along the front surface are plotted on Figure 12. Again, as the value of the normalized crack length approaches 2.5, the ratio becomes constant at a value slightly greater than one. Therefore one of the results of this study is that the transition region ends at a normalized crack length value of 2.5. (Values were not plotted beyond 2.5 because they showed a fairly constant correlation.)

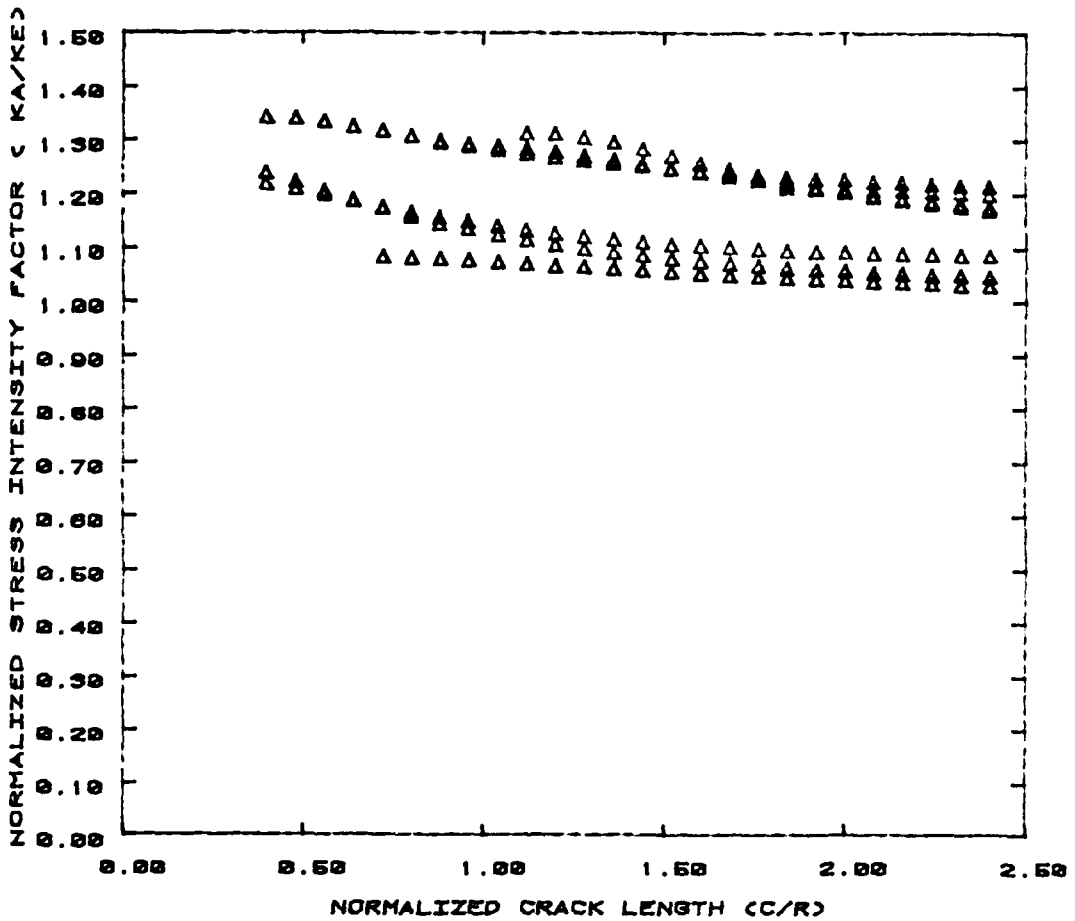

Figure 12: Correlation of Stress Intensity Factors Along the Front Surface of the 7075-T651 Aluminum Tests Until Normalized Crack Length Equals 2.5

VI. Correction Factor Development

6.1 Corner Crack until Back Surface Penetration Region

6.1.1 Correction for Stress Intensity Factor Along the Bore of the Hole. As noted in the previous chapter when the normalized crack depth is approximately equal to 0.75, an apparent step occurs in the correlation plots. This point (a/t = 0.75) will be used as the start of the transition region for both the bore and front surfaces. In developing the correction factor for this region along the bore of the hole, the analytical/experimental correlation was examined in detail. The average value for the correlation fell below unity starting at approximately one half of the way through the material. Using this as a reference point, the correlations were replotted in Figures 13 and 14. From this data the equation for a polynomial regression curve fit was found as

$$(F_{TR})_B = 1/[0.573924 + 1.468068(a/t) - 1.275787(a/t)^2] \qquad (23)$$

and it is plotted in Figures 13 and 14 (in the area where it is to be used). It was found that a second order curve-fit resulted in a good correlation for the data, and kept the number of additional terms to a minimum. Correlations did not improve significantly when higher order curve-fits were attempted.

This correction factor was substituted into the Newman equation by

$$(\Delta K_I)_{COR} = (\Delta K_I)_{NEW} \times (F_{TR})_B \qquad (24)$$

where $(\Delta K_I)_{COR}$ is the corrected stress intensity range and $(\Delta K_I)_{NEW}$ is

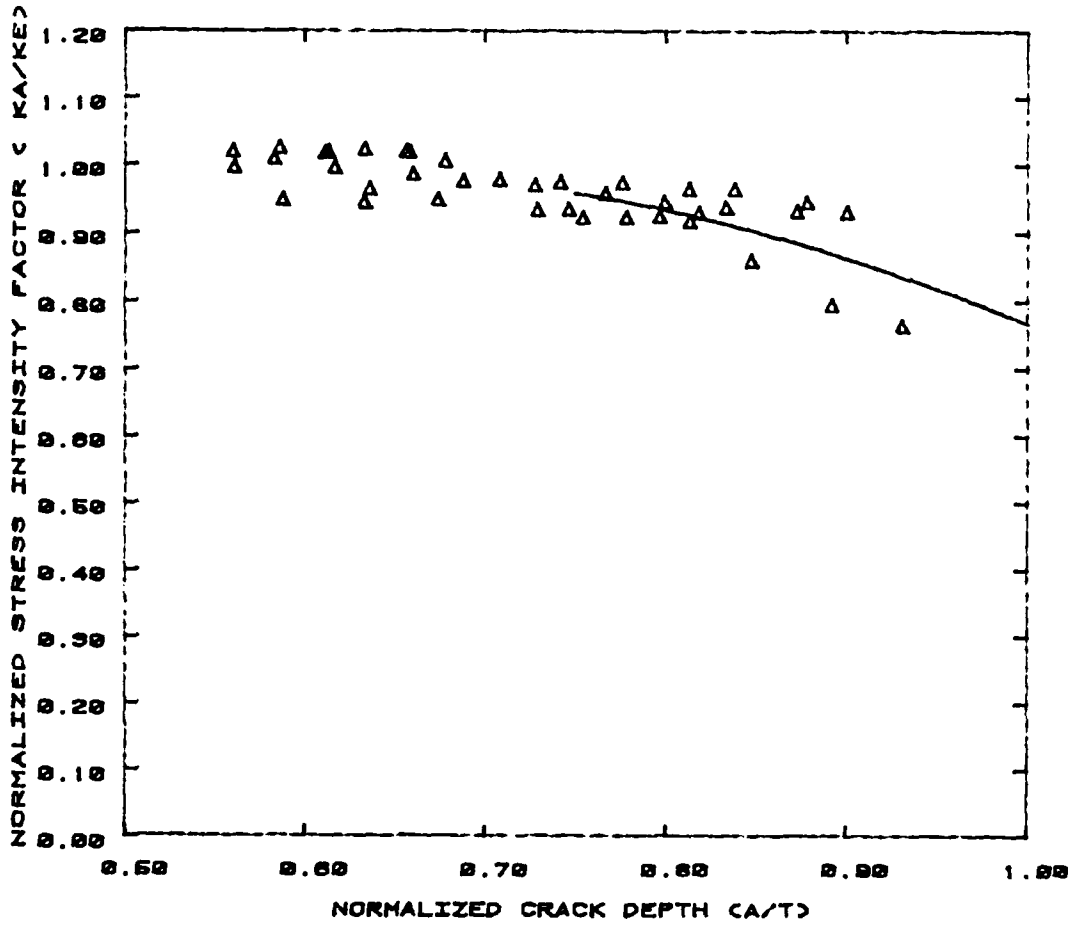

Figure 13: Correlation of Stress Intensity Factors Along the Bore of the Hole in the Region of Interest (Correction Factor Plotted in Transition Region)

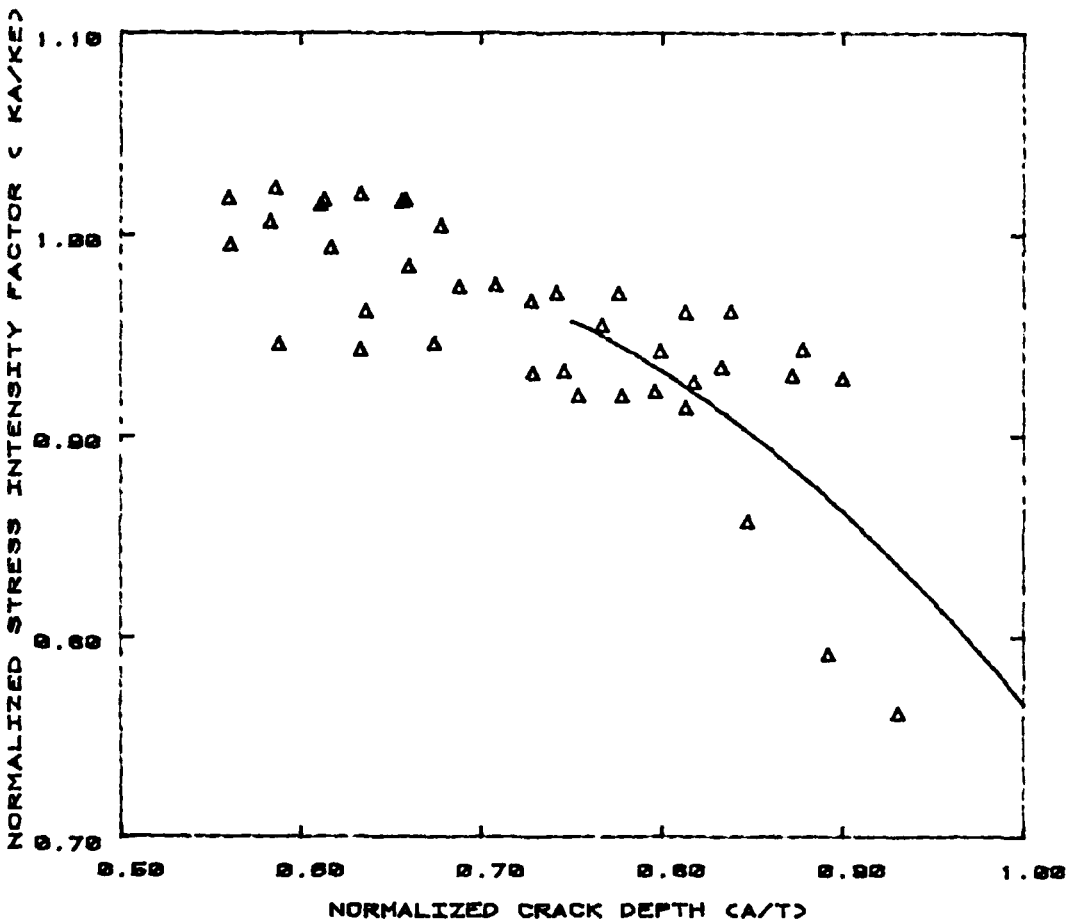

Figure 14: Correlation of Stress Intensity Factors Along the Bore of the Hole in the Region of Interest (Correction Factor Plotted in the Transition Region) (Expanded y-axis)

Newman's solution, a new analytical/experimental correlation was accomplished, which is shown in Figure 15. Since this does not show how accurate the correction factor is, Figure 16 illustrates the relative accuracy by expanding the y-axis of Figure 15. The line illustrates a linear curve fit for the corrected region showing that the desired value of one, or a perfect correlation, is almost satisfied. Figure 17 shows all the data plotted along the bore of the hole and a linear curve fit for that data. This figure shows a slight deviation near the area where normalized crack depth is equal to 0.75, but then shows an improvement in the corrected region. Therefore, the correction factor developed shows a definitely improved correlation in the transition region.

6.1.2 Correction for the Stress Intensity Factor Along the Front Surface. Using the fact that the transition region starts when the normalized crack depth is equal to 0.75, the front surface correlation data was plotted as shown in Figures 18 and 19. Again a polynomial regression curve fit program was used and, in this case, a linear function was found to yield sufficient accuracy. The function used was

$$(F_{TR})_{FS} = 1/[1.316867 - 0.362863(a/t)] \qquad (25)$$

and it is plotted in Figures 18 and 19 (in the area where it is to be used).

After substituting this correction factor, $(F_{TR})_{FS}$, into Equation 24 in place of $(F_{TR})_B$ and then accomplishing the analytical/experimental correlation, the new results are plotted in Figures 20 and 21. These figures demonstrate the relative accuracy in the corrected region. The

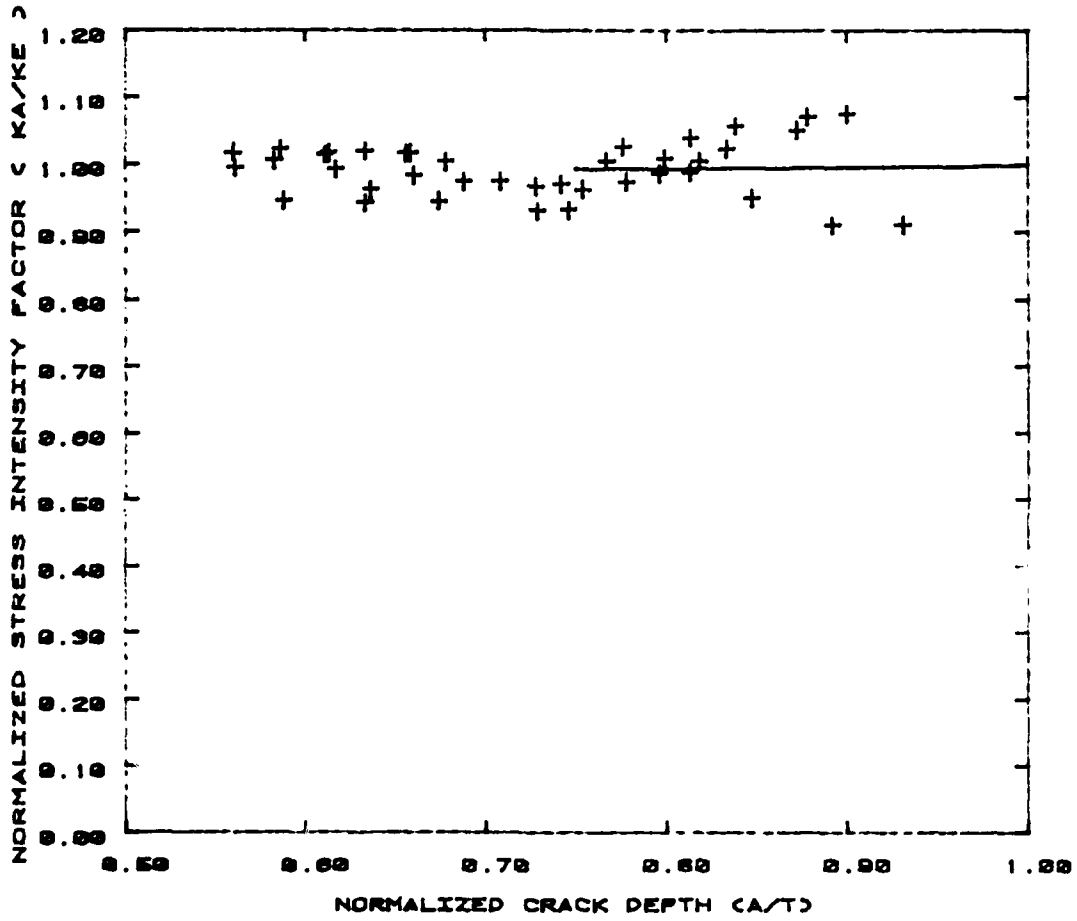

Figure 15: Correlation of Stress Intensity Factors Along the Bore of the Hole in the Region of Interest after Applying the Correction Factor (Best-Fit Linear Function Plotted in the Transition Region)

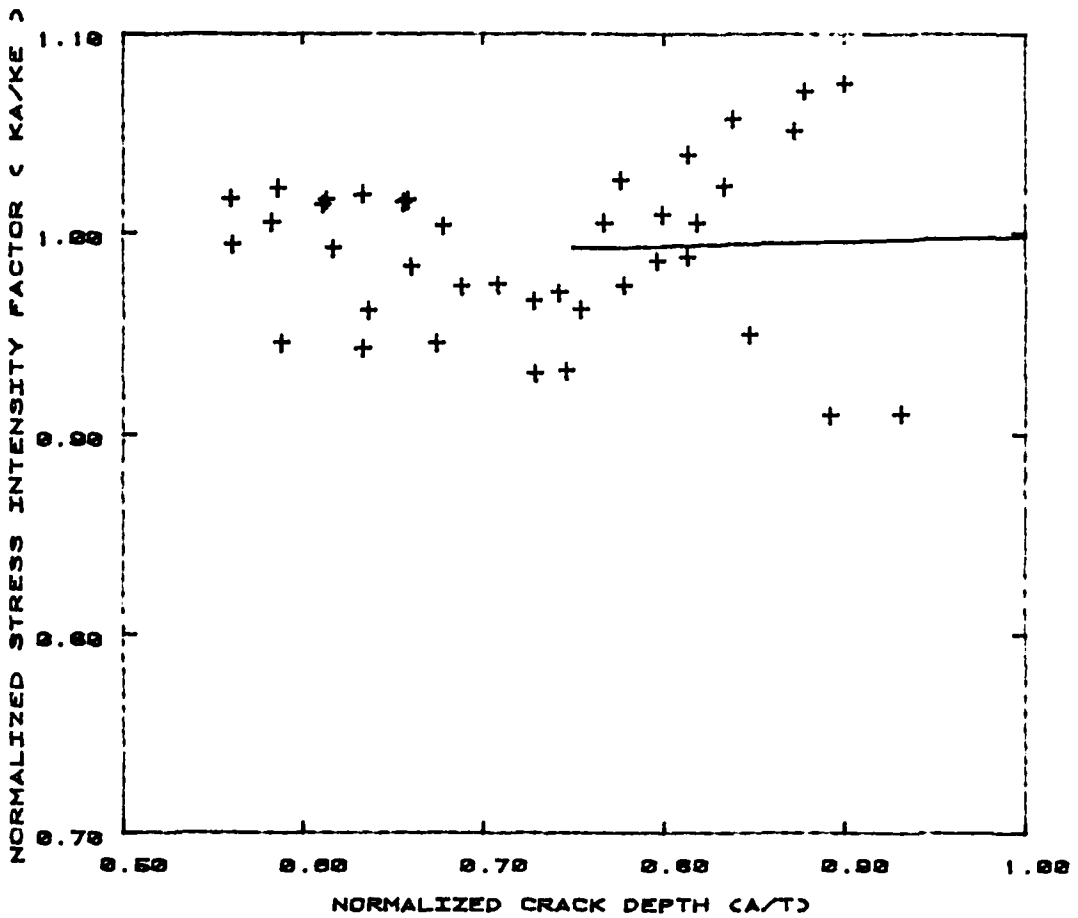

Figure 16: Correlation of Stress Intensity Factors Along the Bore of the Hole in the Region of Interest after Applying the Correction Factor (Best-Fit Linear Function Plotted in Transition Region) (Expanded y-axis)

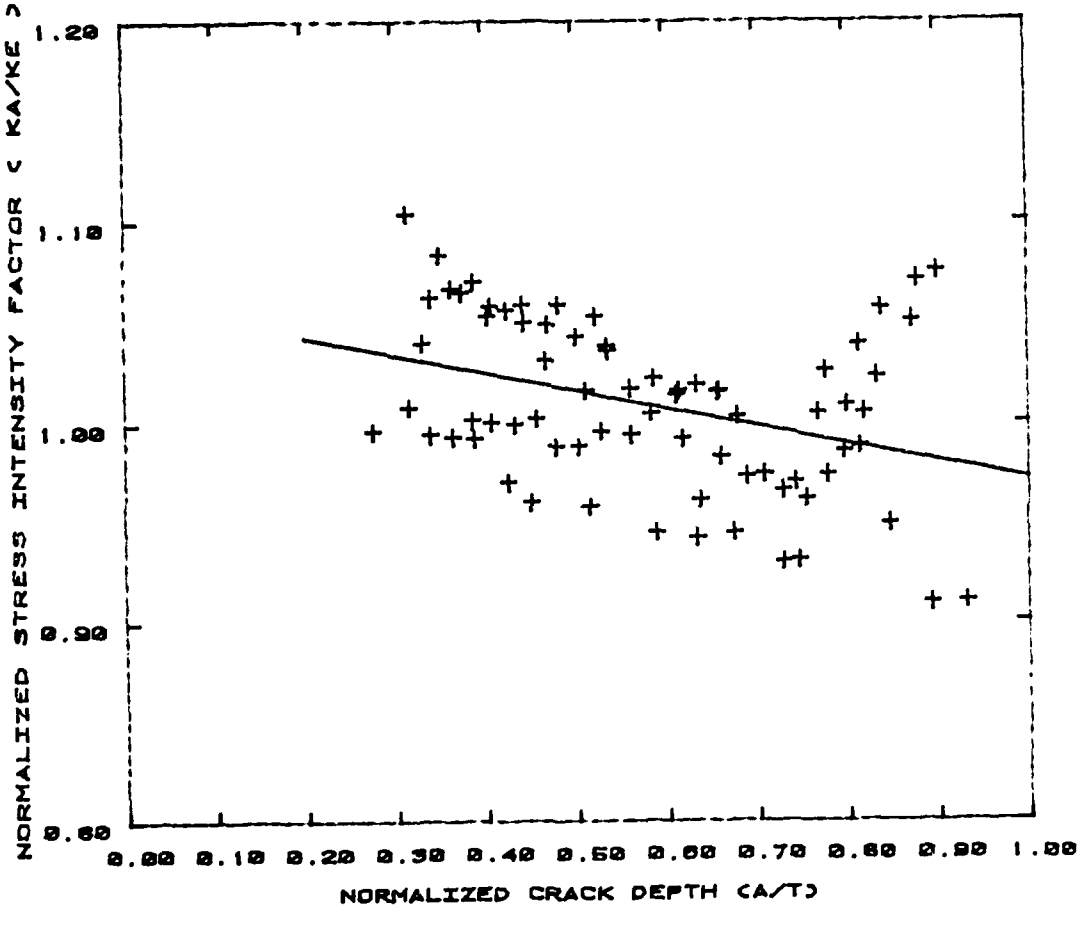

Figure 17: Correlation of Stress Intensity Factors Along the Entire Length of the Bore of the Hole (Best-Fit Linear Function Plotted for Entire Region)

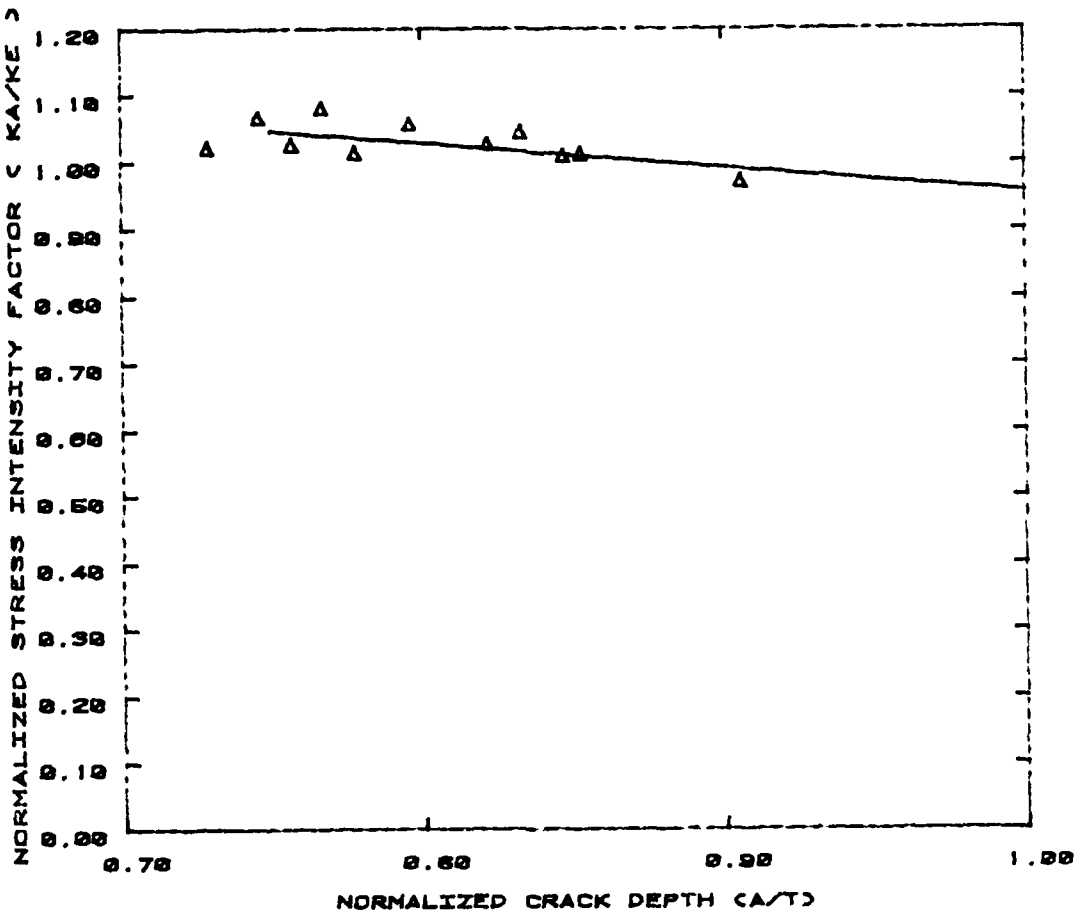

Figure 18: Correlation of Stress Intensity Factors Along the Front Surface of the PMMA Tests in the Region of Interest (Correction Factor Plotted in Transition Region)

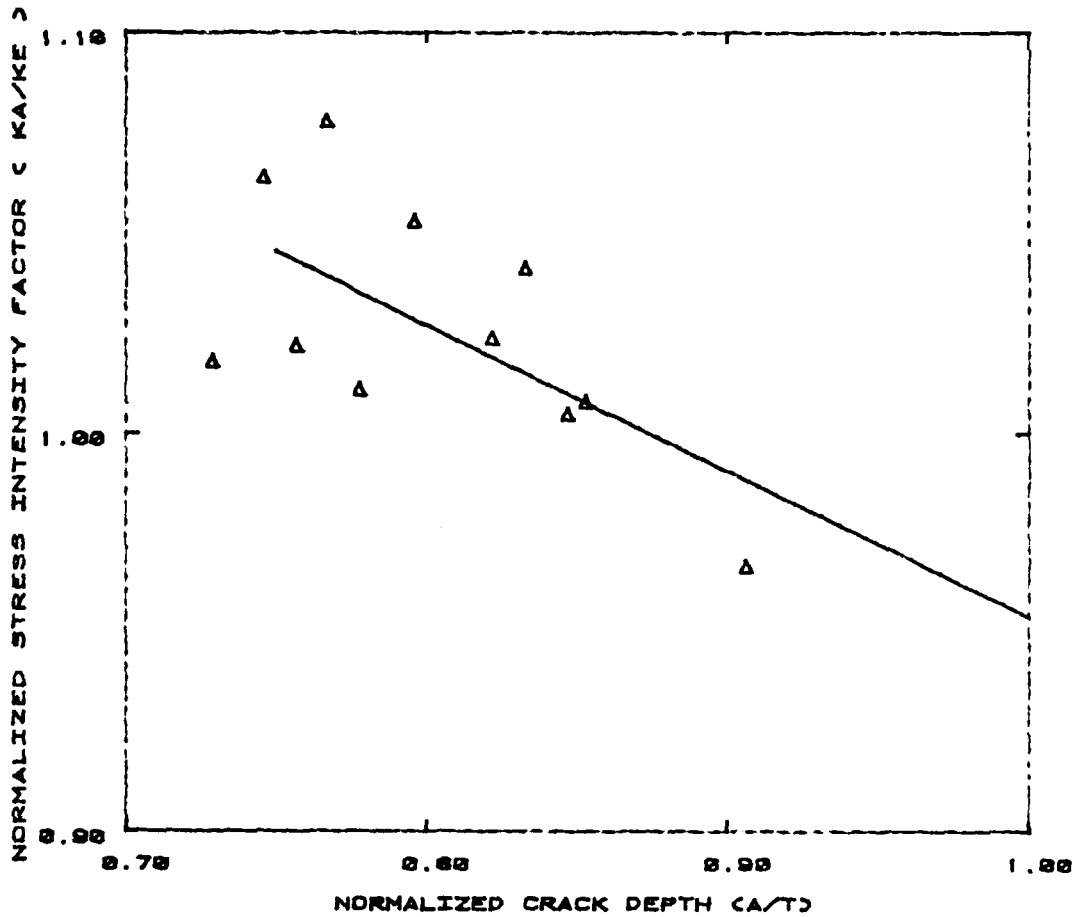

Figure 19: Correlation of Stress Intensity Factors Along the Front Surface of the PMMA Tests in the Region of Interest (Correction Factor Plotted in Transition Region) (Expanded y-axis)

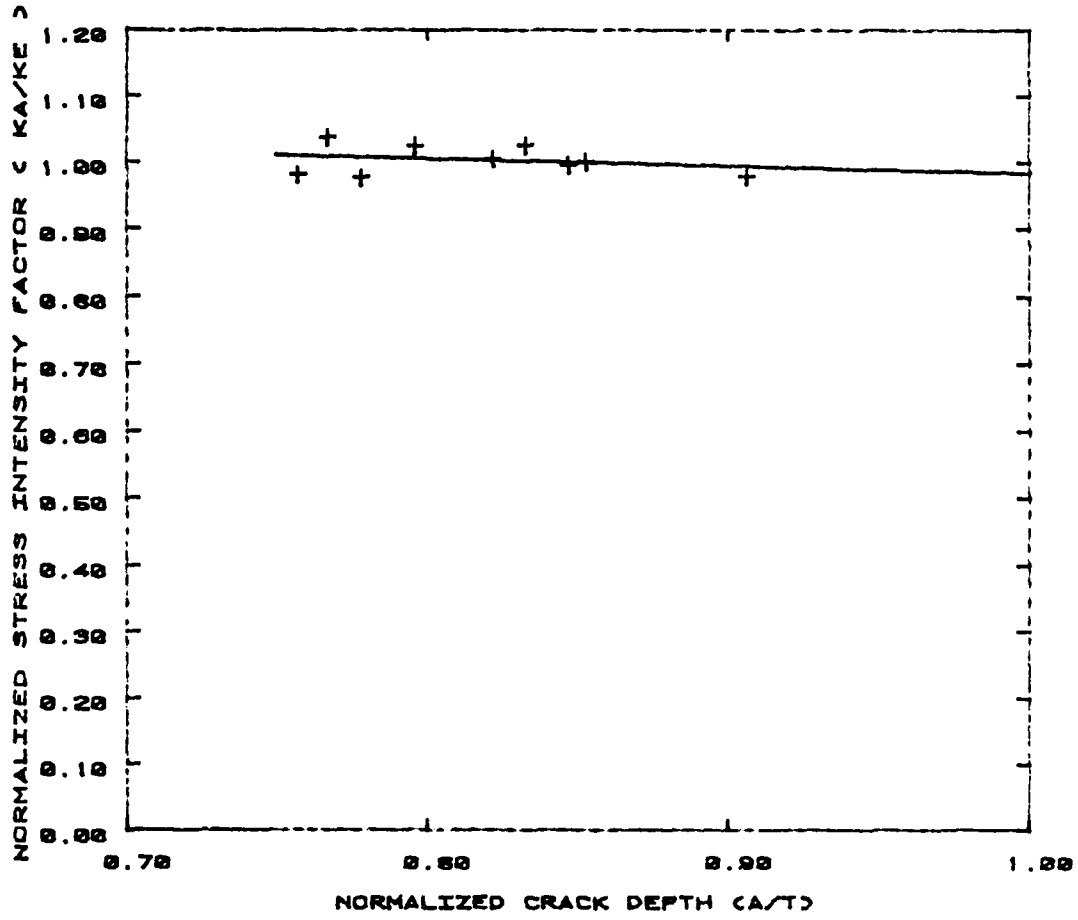

Figure 20: Correlation of Stress Intensity Factors Along the Front Surface of the PMMA Tests in the Region of Interest after Applying the Correction Factor (Best-Fit Linear Function Plotted in Transition Region)

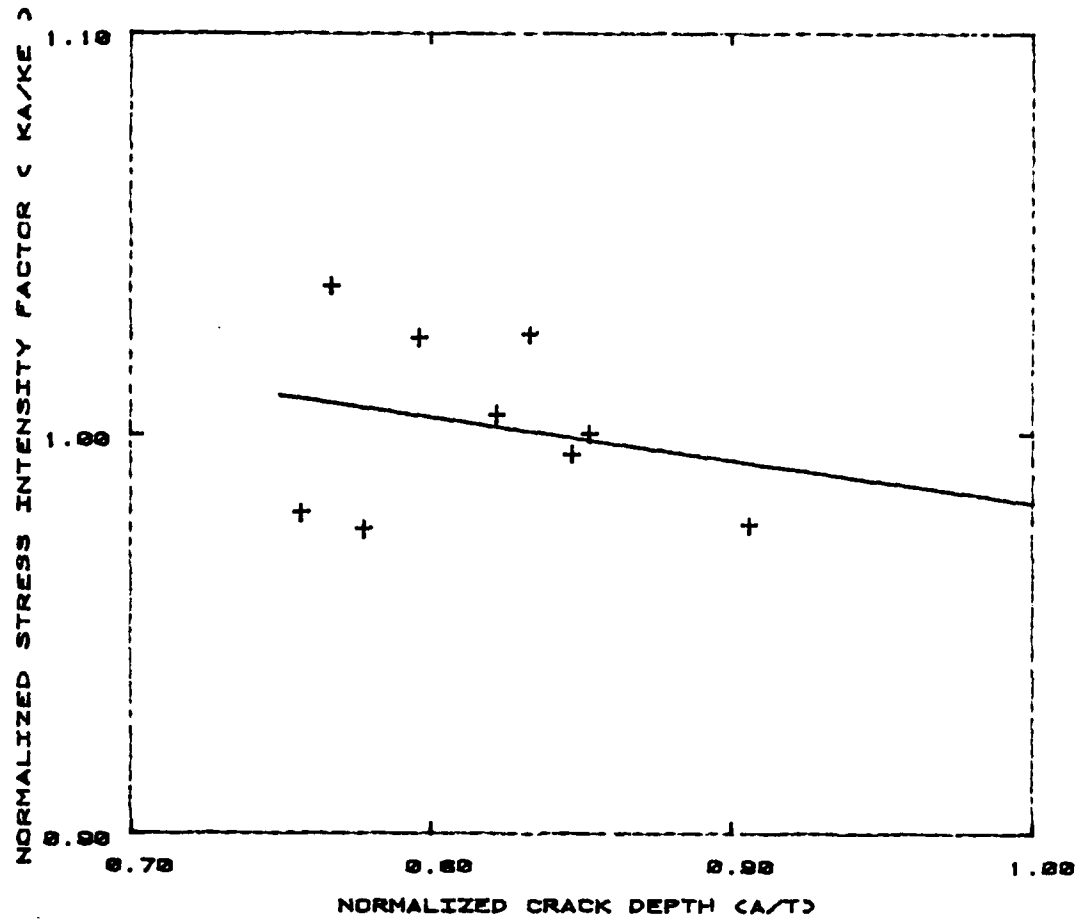

Figure 21: Correlation of Stress Intensity Factors Along the Front Surface of the PMMA Tests in the Region of Interest after Applying the Correction Factor (Best-Fit Linear Function Plotted in Transition Region) (Expanded y-axis)

linear function plotted in Figures 20 and 21 displays the relative accuracy of this correction factor. Figure 22 contains all the surface data and a linear curve fit for the entire front surface. This linear function presents an excellent correlation for the stress intensity ranges on the front surface.

6.2 Back Surface Penetration until Final Fracture Region

6.2.1 Correction for Stress Intensity Factor Along the Back Surface. As noted in the previous chapter, the correlations tend to become constant at a normalized crack length of 2.5. Figure 23 displays the correlation for the back surface. The polynomial regression curve fit used for this data is

$$(F_{TR})_{BS} = 1/[0.191601 + 0.724961(c'/R) - 0.158451(c'/R)^2] \quad (26)$$

and it is plotted in Figure 23 in its effective region. Due to the use of the seven point incremental technique to compute the crack growth rate, actual data could not be obtained for values of the normalized crack length less than approximately 0.8 for this surface. This causes the correction factor to be extrapolated in the region from 0.8 to 0.0. However, since the crack growth rate in this area is very high, the amount of time spent in this region should have minimal influence on the total life of the specimen.

Substituting this correction factor, $(F_{TR})_{BS}$, into Equation 24 for $(F_{TR})_B$ and replacing Newman's equation with Bowie's equation, the newly corrected analytical stress intensity factor ranges are found. These results are similar to those demonstrated previously.

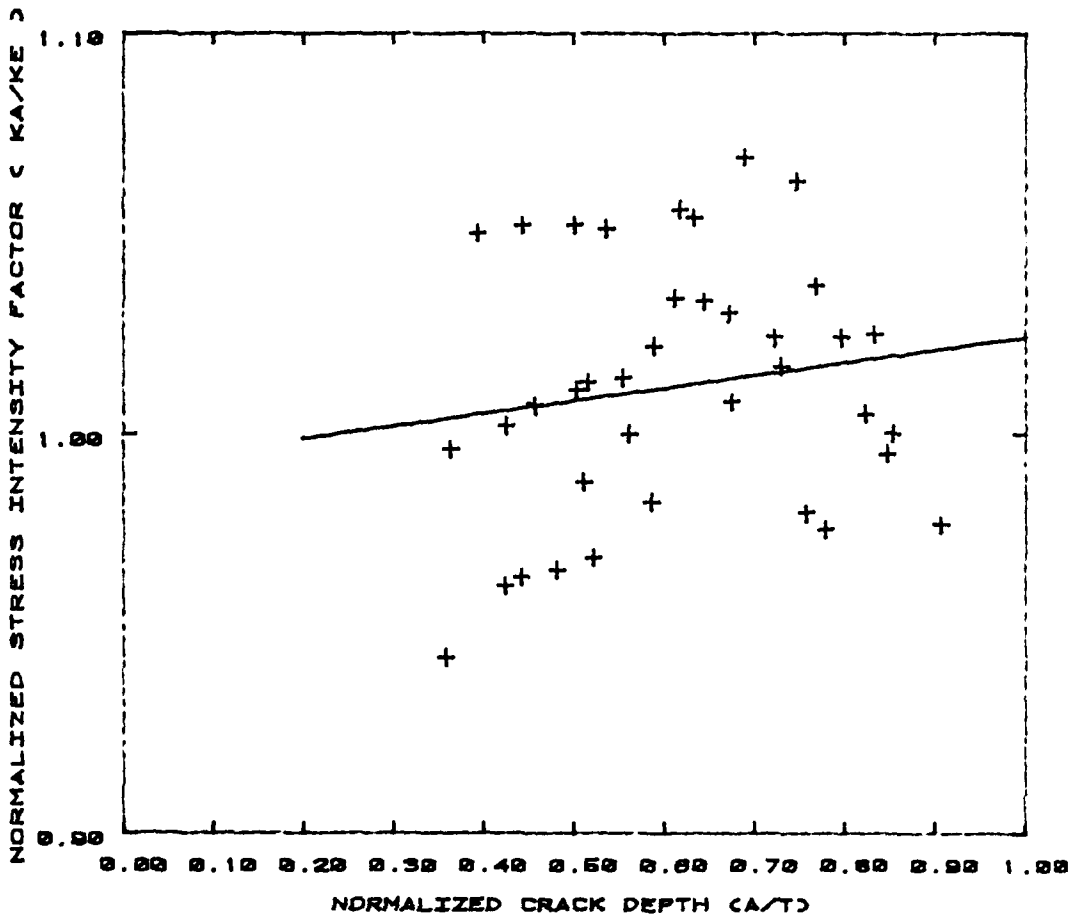

Figure 22: Correlation of Stress Intensity Factors Along the Front Surface of the PMMA Tests after Applying the Correction Factor (Best-Fit Linear Function Plotted for Entire Region)

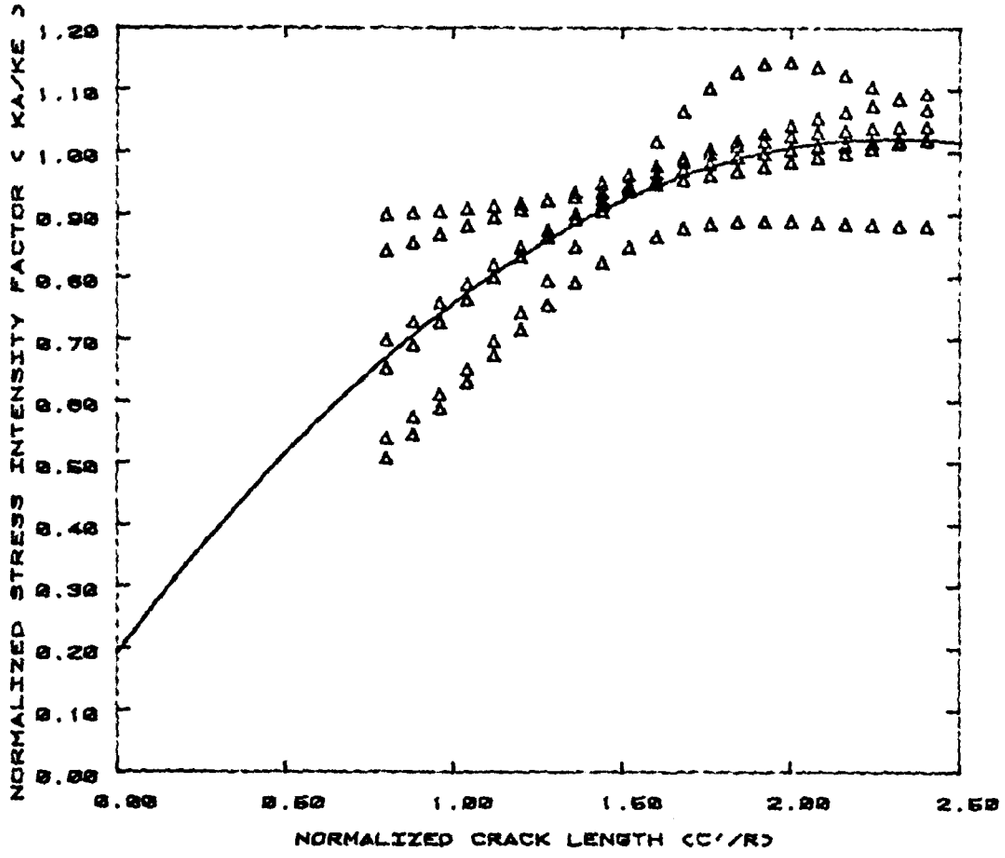

Figure 23: Correlation of Stress Intensity Factors Along the Back Surface of the 7075-T651 Aluminum Tests in the Region of Interest (Correction Factor Plotted in Transition Region)

6.2.2 Correction for Stress Intensity Factor Along the Front Surface. Figure 24 illustrates the correlation of surface stress intensity factor ranges in the same region used for the back surface correction. One difference between the front and back surface is that data along the front surface were recorded for the entire experiment which allowed actual results to be plotted from a minimum normalized crack length of approximately 0.5 rather than 0.8, which was used for the back surface. The polynomial regression curve fit for the data is

$$(F_{TR})_{FS} = 1/[1.279537 - 0.106745(c/R) + 0.018451(c/R)^2] \qquad (27)$$

and the results are shown in Figure 24 in the effective region. By substituting this correction factor into Equation 24 and using Bowie's equation rather than Newman's, the new correlations are found. These again show a much better correlation pattern.

6.3 Back Surface Crack Length as a Function of Front Surface Crack Length

Since in most applications it is not possible to measure the crack length on both surfaces, the capability to calculate the crack length on both surfaces knowing only the crack length on one surface is extremely desirable. In most cases only the front surface crack length is measured, thus the back surface crack length should be expressed as a function of the front surface crack length. Figure 25 shows the correlation between front and back surface crack lengths. In this figure the normalized crack lengths are plotted using the front surface

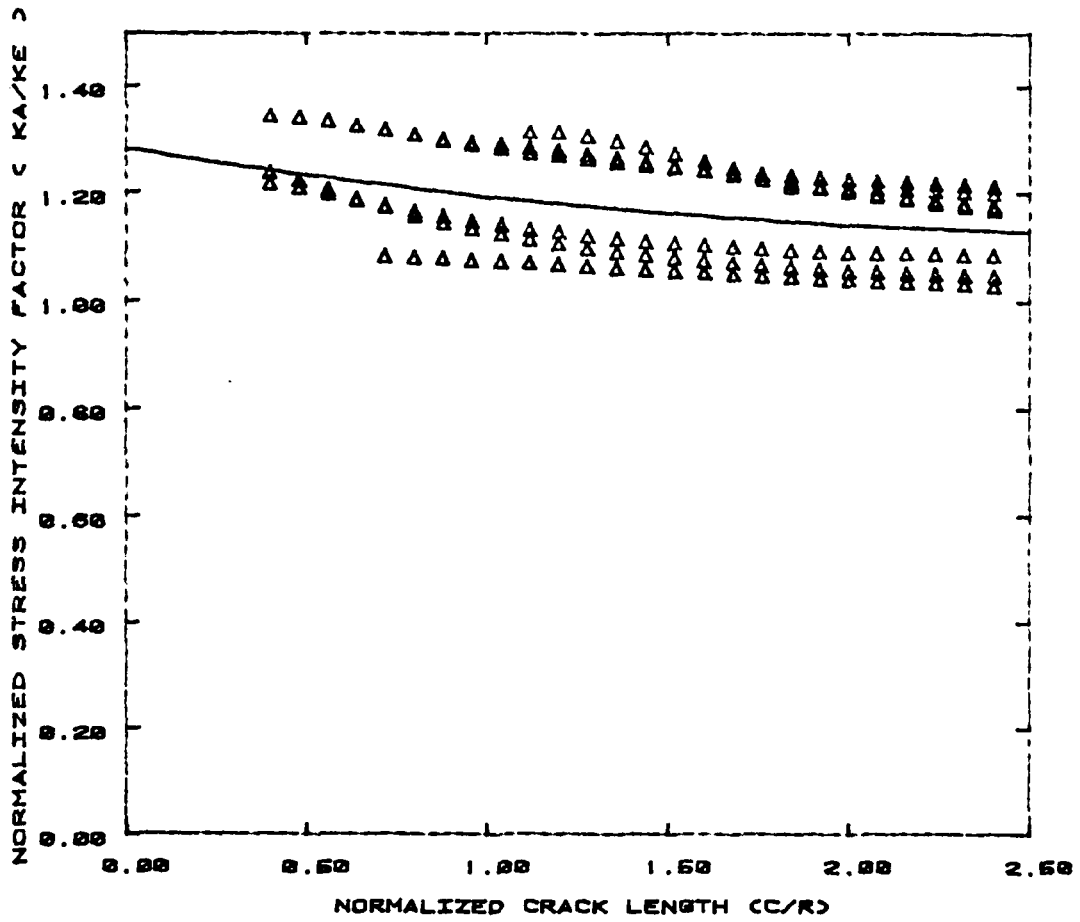

Figure 24: Correlation of Stress Intensity Factors Along the Front Surface of the 7075-T651 Aluminum Tests in the Region of Interest (Correction Factor Plotted in Transition Region)

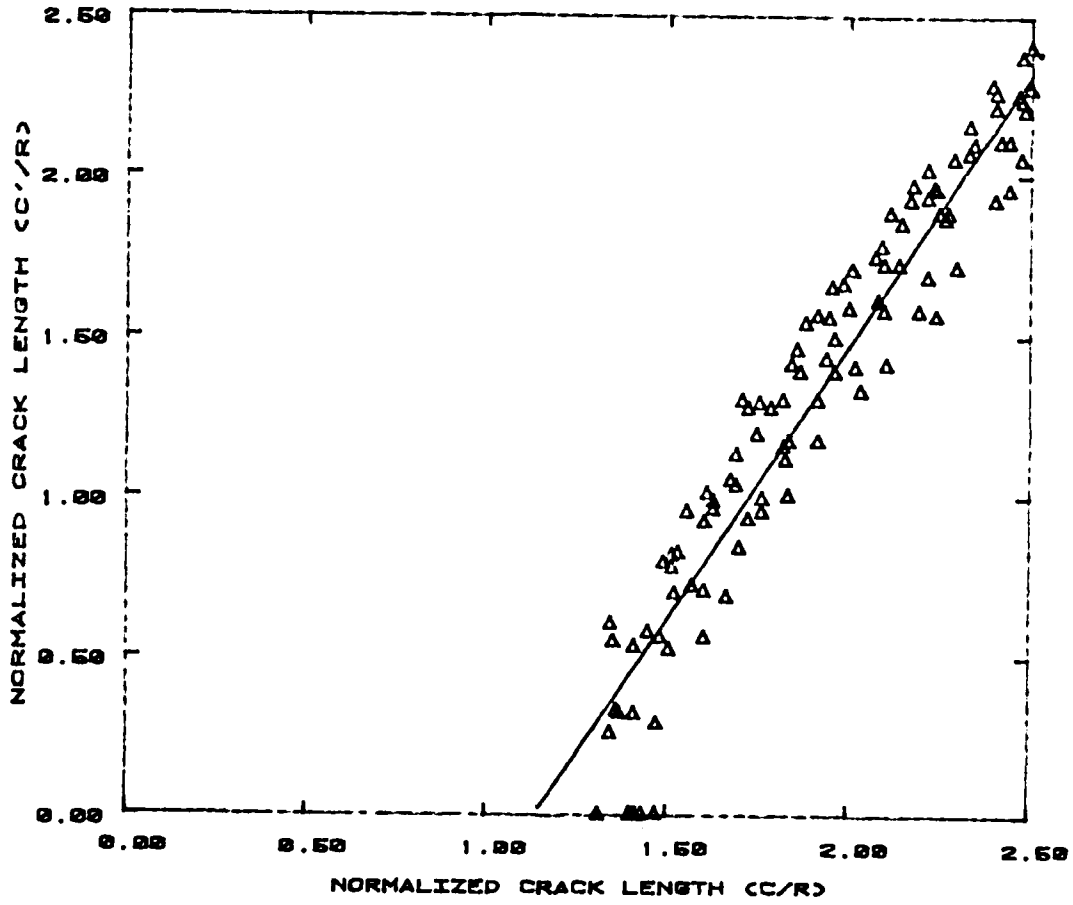

Figure 25: Relationship of the Normalized Back Surface Crack Length as a Function of the Normalized Front Surface Crack Length (Best-Fit Relationship Plotted)

crack length as the independent variable. The linear relationship which best fits the data is

$$c'/R = -1.9311 + 1.70076(c/R) \tag{28}$$

and it is plotted in Figure 25. Using this relationship the corrected stress intensity factor ranges can be calculated on both the front and back surfaces knowing only the front surface crack length after back surface penetration, either predicted or actual. This function is only valid in the region from back surface penetration until the normalized crack length is 2.5, which is similar to the region used for the front and back surface correction factors (see Section 6.2).

VII. Life and Crack Shape Predictions and Comparisons

7.1 Life Predictions Based upon Corrected Stress Intensity Factors

Life predictions were made for corner-cracked specimens subjected to constant amplitude loading. The procedure used was to calculate the stress intensity factor range and then to obtain the crack growth rate using Walker's equation (see Eqn 2)

$$dc/dN = C[\Delta K(1 - R)^m]^n \ . \tag{29}$$

Here, C, m, and n are the material constants, as given in Section 3.2 for 7075-T651 Aluminum. After calculating the crack growth rate, the new crack length was found by integrating after each cycle and adding the change in crack length to the previous crack length.

The life predictions for the seven experiments conducted are presented in Table 5 along with the actual experimental results. These results show an average life prediction of 78.85 percent of the actual life. The average prediction from crack initiation to back surface penetration was 65.76 percent of the experimental results, while the average prediction from back surface penetration to final fracture was 86.84 percent. Of the seven cases one test was slightly unconservative, with a 101.24 percent total life prediction and a 110.55 percent prediction for back surface penetration to final fracture. The range for total life predictions was 63.37 to 101.24 percent of the actual values. For crack initiation to back surface penetration, the range was 44.71 to 95.74, and for back surface penetration to final fracture, the range was 69.38 to 110.55 percent. To examine the effectiveness of this

		SPECIMENS							
		R=0.1 σ_{max}=20	R=0.1 σ_{max}=15	R=0.3 σ_{max}=20	R=0.3 σ_{max}=15	R=-.3 σ_{max}=15	R=-.5 σ_{max}=20	R=-.5 σ_{max}=15	AVERAGE
ACTUAL	a=t	7980	12780	13600	14510	8450	6390	13410	
	$c=c_c$	19240	41960	32100	54360	27030	15740	42290	
	$a=t \rightarrow c=c_c$	11260	29180	18500	39850	18580	9350	28880	
CORRECTED (PREDICTED/ACTUAL PERCENTAGE)	a=t	3955 (49.56)	9815 (76.80)	6080 (44.71)	13892 (95.74)	6823 (80.75)	3530 (55.24)	7717 (57.55)	65.76
	$c=c_c$	13211 (68.66)	34696 (82.69)	20343 (63.37)	52346 (96.30)	27364 (101.24)	11653 (74.03)	27753 (65.63)	78.85
	$a=t \rightarrow c=c_c$	9256 (82.20)	24881 (85.27)	14263 (77.10)	38454 (96.50)	20541 (110.55)	8123 (86.88)	20036 (69.38)	86.84

TABLE 5: CORRECTED MODEL LIFE PREDICTIONS

approach, two other models, proposed earlier (25, 26), were tested and the results obtained are discussed in the following section.

7.2 Life Predictions Based on Other Models

7.2.1 Newman-Bowie Method. The Newman-Bowie method was used as presented by Engle (26) to predict the fatigue life for the specimens considered in the previous section. This method ignores the transition region, i.e. it assumes a through-the-thickness crack once back surface penetration has occurred. Results were obtained using the procedure of Section 7.1, and they are presented in Table 6. The average life prediction was 69.32 percent of the experimental results, with a range of 55.18 to 90.44. The life prediction from crack initiation to back surface penetration ranged from 48.72 to 105.95 percent, with an average of 71.97. For the region from back surface penetration until final fracture, the average prediction was 69.12 percent, ranging from 57.31 to 91.25. These results will be compared to the ones obtained from the corrected approach in Section 7.4.

7.2.2 Brussat Method. Since the Brussat method (25) was developed for a quarter-circular crack, the initial crack length used was the average of the initial crack lengths along the bore of the hole and along the surface. The procedure used was the same as that outlined in Section 7.1, except for calculating the stress intensity factor ranges where the following equation from Brussat's report (25) was used,

$$\Delta K_I = \Delta S\sqrt{\pi c}\, f_w\, f_{TR} \,. \tag{30}$$

		SPECIMENS							
		R=0.1 σ_{max}=20	R=0.1 σ_{max}=15	R=0.3 σ_{max}=20	R=0.3 σ_{max}=15	R=-.3 σ_{max}=15	R=-.5 σ_{max}=20	R=-.5 σ_{max}=15	AVERAGE
ACTUAL	a=t	7980	12780	13600	14510	8450	6390	13410	
	$c=c_c$	19240	41960	32100	54360	27030	15740	42290	
	$a=t \rightarrow c=c_c$	11260	29180	18500	39850	18580	9350	28880	
NEWMAN-BOWIE (PREDICTED/ACTUAL PERCENTAGE)	a=t	4311 (54.02)	10771 (84.28)	6626 (48.72)	15373 (105.95)	7491 (88.65)	3815 (59.70)	8374 (62.45)	71.97
	$c=c_c$	11503 (59.79)	30066 (71.65)	17714 (55.18)	45113 (82.99)	24445 (90.44)	10427 (66.25)	24924 (58.94)	69.32
	$a=t \rightarrow c=c_c$	7192 (63.87)	19295 (66.12)	11088 (59.94)	29740 (74.63)	16954 (91.25)	6612 (70.72)	16550 (57.31)	69.12

TABLE 6: NEWMAN-BOWIE MODEL LIFE PREDICTIONS

Here,

$$f_{TR} = 1 - [0.2886/(1 + 2(c/t)^2)] \tag{31}$$

and ΔS and f_w are as defined in Equations 8 and 19.

Life predictions are tabulated in Table 7. The averages for total life, crack initiation until back surface penetration, and back surface penetration to final fracture are 100.40, 149.13, and 77.07 percent, respectively. The predictions for total life range from 82.71 to 124.89 percent, while for the region from crack initiation until back surface penetration the range is 103.51 to 226.57 percent, and finally, for the region from back surface penetration to final fracture the values range from 64.72 to 101.85 percent. These results will also be compared to those obtained by the Newman-Bowie method and the corrected method in Section 7.4.

7.3 Crack Shape Predictions

The actual crack shape at back surface penetration along with the predicted crack shapes for the three models discussed previously are presented in Table 8. The Newman - Bowie Model has an average prediction of 104.89 percent when compared to the actual results, while the corrected method has an average of 108.94 percent. The Brussat solution assumes that the crack is quarter-circular. The result of this assumption is that the crack shape will always be equal to one. This yields an average prediction of 70.25 percent. These crack shape predictions will be compared in the next section.

		SPECIMENS							
		R=0.1 σ_{max}=20	R=0.1 σ_{max}=15	R=0.3 σ_{max}=20	R=0.3 σ_{max}=15	R=-.3 σ_{max}=15	R=-.5 σ_{max}=20	R=-.5 σ_{max}=15	AVERAGE
ACTUAL	a=t	7980	12780	13600	14510	8450	6390	13410	
	$c=c_c$	19240	41960	32100	54360	27030	15740	42290	
	$a=t \rightarrow c=c_c$	11260	29180	18500	39850	18580	9350	28880	
BRUSSAT (PREDICTED/ACTUAL PERCENTAGE)	a=t	9684 (121.35)	22929 (179.41)	14077 (103.51)	32875 (226.57)	14833 (175.53)	7386 (115.59)	16350 (121.92)	149.13
	$c=c_c$	17310 (89.97)	44556 (106.19)	26550 (82.71)	66004 (121.42)	33757 (124.89)	14917 (94.77)	35041 (82.86)	100.40
	$a=t \rightarrow c=c_c$	7626 (67.73)	21627 (74.12)	12473 (67.42)	33129 (83.13)	18924 (101.85)	7531 (80.55)	18691 (64.72)	77.07

TABLE 7: BRUSSAT MODEL LIFE PREDICTIONS

	SPECIMENS							
	R=0.1 σ_{max}=20	R=0.1 σ_{max}=15	R=0.3 σ_{max}=20	R=0.3 σ_{max}=15	R=-.3 σ_{max}=15	R=-.5 σ_{max}=20	R=-.5 σ_{max}=15	AVERAGE
ACTUAL	1.28	1.53	1.41	1.50	1.36	1.31	1.51	
NEWMAN-BOWIE (PREDICTED/ACTUAL PERCENTAGE)	1.442 (112.66)	1.526 (99.74)	1.466 (103.97)	1.549 (103.27)	1.460 (107.35)	1.448 (110.53)	1.460 (96.69)	104.89
CORRECTED (PREDICTED/ACTUAL PERCENTAGE)	1.519 (118.67)	1.542 (100.78)	1.530 (108.51)	1.578 (105.20)	1.563 (114.93)	1.528 (116.64)	1.478 (97.88)	108.94

TABLE 8: FINAL CRACK SHAPE PREDICTIONS AT BACK SURFACE PENETRATION

7.4 Comparisons

Since Brussat's Method is for a quarter-circular flaw, the accuracy of his average total life prediction is outstanding. However, as shown in Table 7, in eleven out of twenty-one predictions his approach is unconservative. Due to this fact, this solution will not be discussed further.

The corrected method yields a 13.75 percent improvement in total life prediction, and a 25.64 percent improvement in life prediction for the region from back surface penetration to final fracture over the Newman-Bowie approach. However, the corrected method is 8.63 percent more conservative in the region from crack initiation to back surface penetration. Clearly, the corrected approach yields better results both in total life and in the region from back surface penetration to final fracture; however, it is slightly more conservative (8.63 percent) in the region from crack initiation to back surface penetration. This peculiarity deserves a more detailed explanation.

In the transition region, the region from normalized crack depth of 0.75 to 1.0, the Newman - Bowie solution is very unconservative in comparison with the corrected model, as shown in Figure 26. This leads to a prediction of more cycles than actually occur, which in turn increases the overall average prediction for each test. The average life prediction between the normalized crack depths of 0.75 and 1 for the corrected model is 69.44 percent, while the average for the Newman-Bowie model is 111.14 percent. This difference accounts for the corrected model being slightly more conservative for the region from crack initiation to back surface penetration.

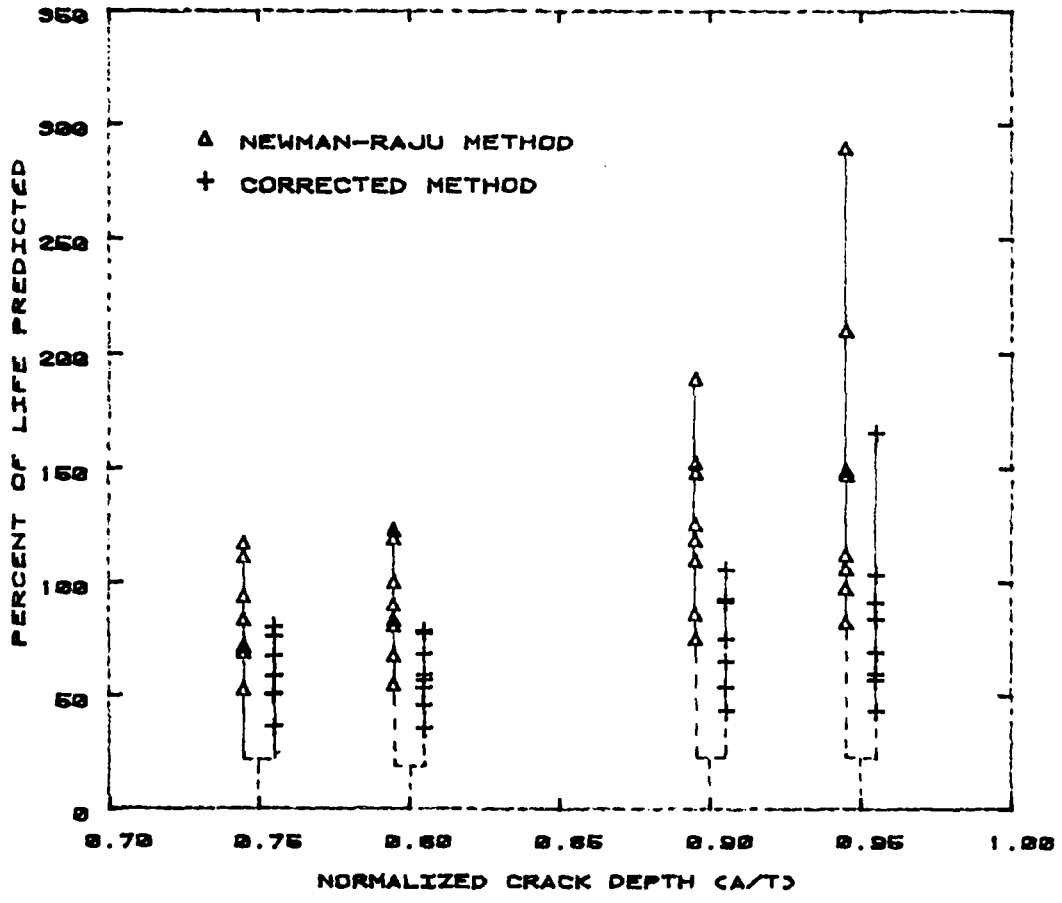

Figure 26: Percent of Life Predicted by Corrected Model and by Newman-Raju Model in the Transition Region at Specific Points

As noted in Section 7.3, the comparison between the Brussat solution for a quarter-circular flaw and the other two models, which are based on elliptical flaws, is unrealistic; in all the tests completed the final crack shapes tend to be more elliptical than circular. When comparing crack shapes for the other models, it is found that the corrected model is slightly more conservative than the Newman-Bowie approach. This is due to the fact that the corrected model predicts accelerated crack growth along the bore of the hole, but this affects only slightly the crack growth on the surface. An interesting point should be made here. The crack lengths along the surface of the aluminum specimens are the measured values, which do not account for any pinning action on the surface. As was noted in Section 3.2, in the PMMA specimens, extrapolated crack lengths, which attempted to account for this pinning action, are 3 to 18 percent longer than the measured results. This pinning action, not considered in the aluminum specimens, could be responsible for most of the difference between the actual crack shape and the predicted values.

VIII. Conclusions and Recommentations

The Newman corner crack solution (14) and the Grandt linearization of the Bowie through-crack solution (26) accurately predict the stress intensity factor range for a corner crack emanating from a hole as it grows until it reaches final fracture. However, in a region near where the corner crack penetrates the back surface and slightly beyond, these models are very inaccurate. This transition region, i.e. the area just prior to the penetration of the back surface by the corner crack and until the crack becomes a through-the-thickness one, was found to start when the normalized crack depth (a/t) was 0.75, and end when the normalized crack length (c/R) reached 2.5. This was accomplished by plotting analytical/experimental correlations.

From these correlation plots, correction factors were found for the transition region. After applying the correction factors to Newman's and the Grandt-Bowie's solutions in the region defined previously, a much better prediction of the stress intensity factor ranges was obtained throughout the transition region. This improvement in the prediction of stress intensity factor ranges improved the total life prediction of test specimens by almost 15 percent. This improvement is vital in the development of accurate life predictions for structural components.

This study has demonstrated that the proposed corrections to the currently used stress intensity factor models have resulted in significantly better life predictions for constant amplitude loading. Since these correction factors were developed using non-dimensional

terms, further tests should be conduted using varying thicknesses and radii to verify these results. The correction factors to the Newman-Raju solution are limited to cases where the initial crack eccentricity, a/c, is greater than one. Future studies should determine if correction factors are required for the case when the crack eccentricity is less than one. These results are material independent, as demonstrated by the use of the correction factors developed from PMMA for the aluminum tests. After these correction factors are verified by further testing using spectrum loading, they should be considered for incorporation into the Air Force Damage Tolerant Design Handbook (2).

Appendix: Crack Growth Rate Plots

The following figures show the crack growth rate as a function of crack length for the 7075-T651 Aluminum specimens. The first seven display the crack growth rate for the back surface, and the final seven show the crack growth rate for the front surface. Each figure shows the data for the two test specimens under each load condition, and a least squares curve-fit to the data. These curve-fits are used in Section 3.2 to obtain the experimental stress intensity factor ranges.

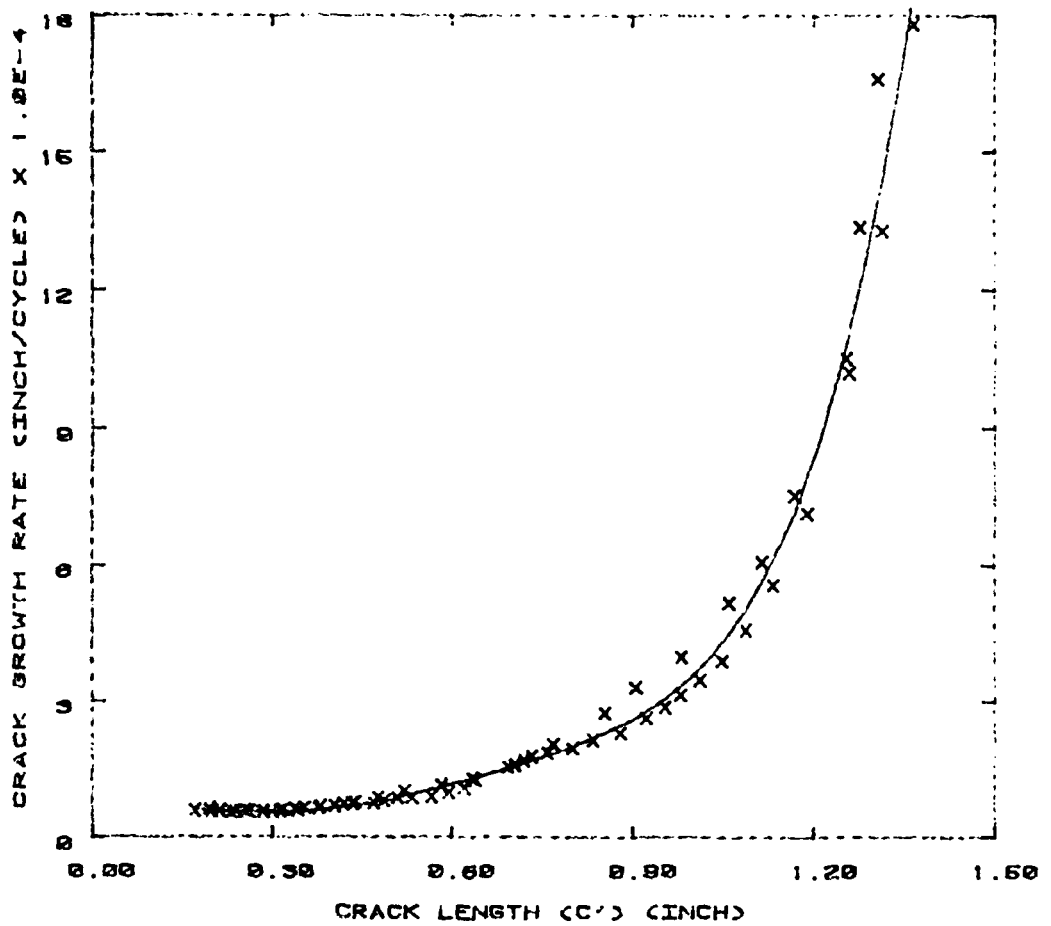

Figure A-1: Crack Growth Rate for the Back Surface of 7075-T651 Aluminum Specimens with a Maximum Stress of 20 and a Load Ratio of 0.] as a function of Crack Length

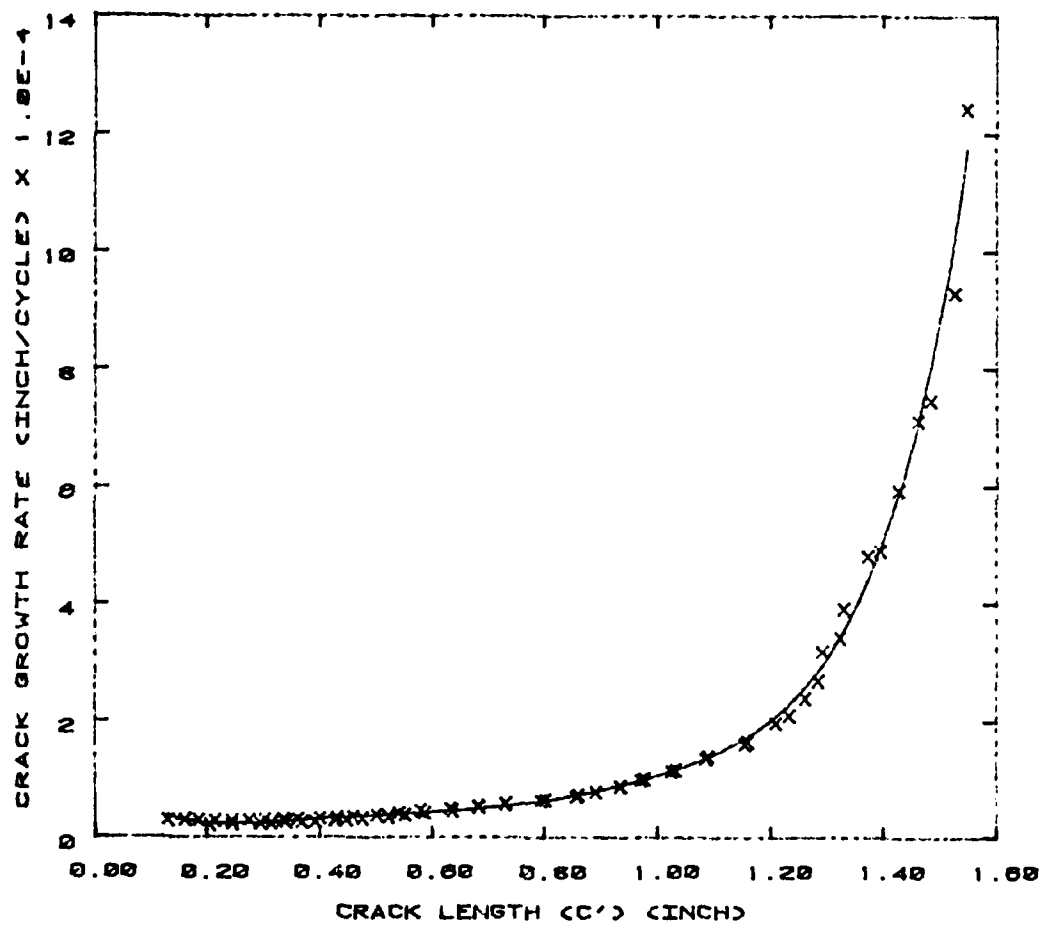

Figure A-2: Crack Growth Rate for the Back Surface of 7075-T651 Aluminum Specimens with a Maximum Stress of 15 and a Load Ratio of 0.1 as a Function of Crack Length

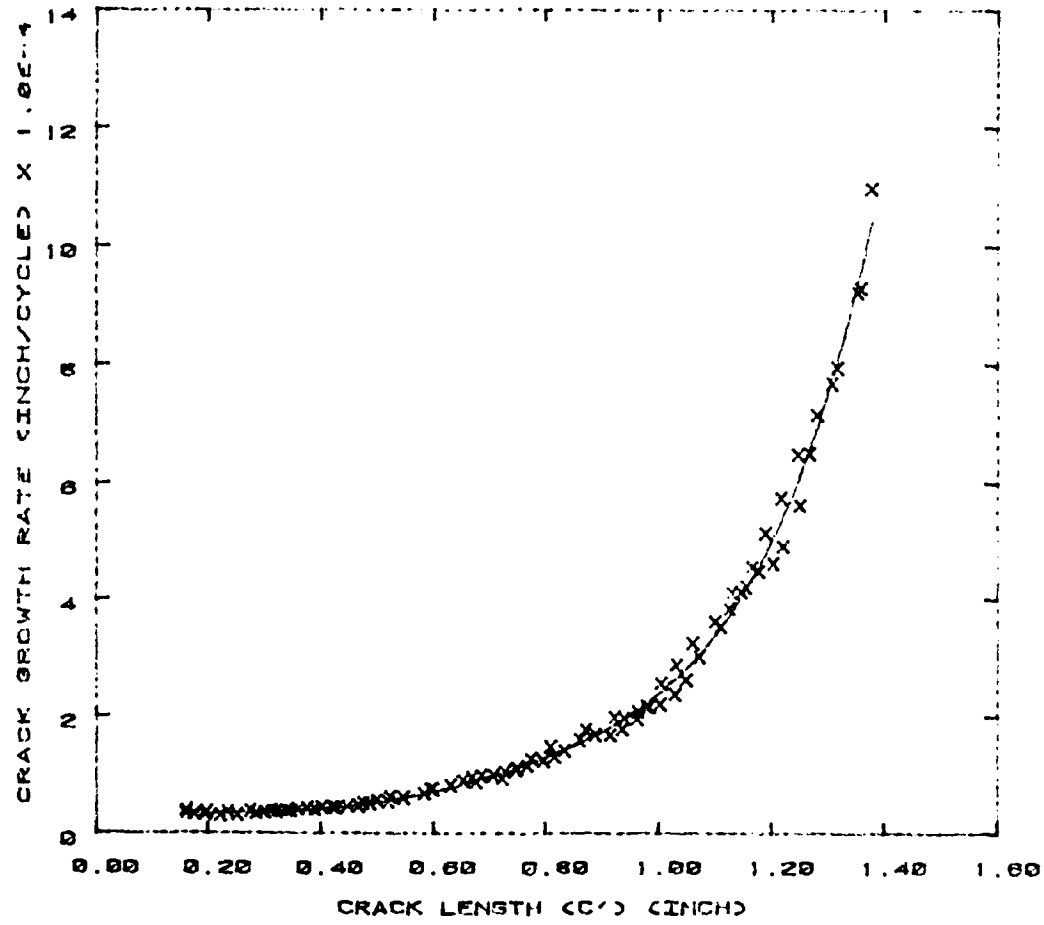

Figure A-3: Crack Growth Rate for the Back Surface of 7075-T651 Aluminum Specimens with a Maximum Stress of 20 and a Load Ratio of 0.3 as a Function of Crack Length

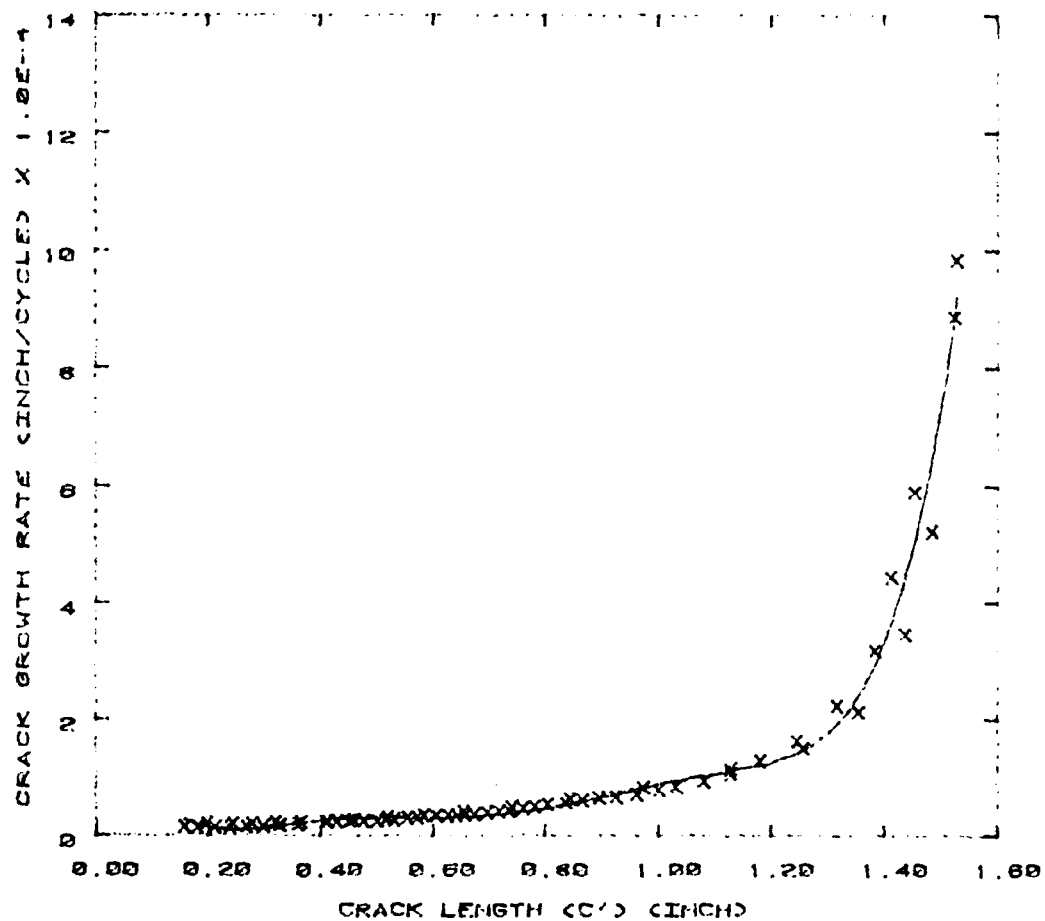

Figure A-4: Crack Growth Rate for the Back Surface of 7075-T651 Aluminum Specimens with a Maximum Stress of 15 and a Load Ratio of 0.3 as a Function of Crack Length

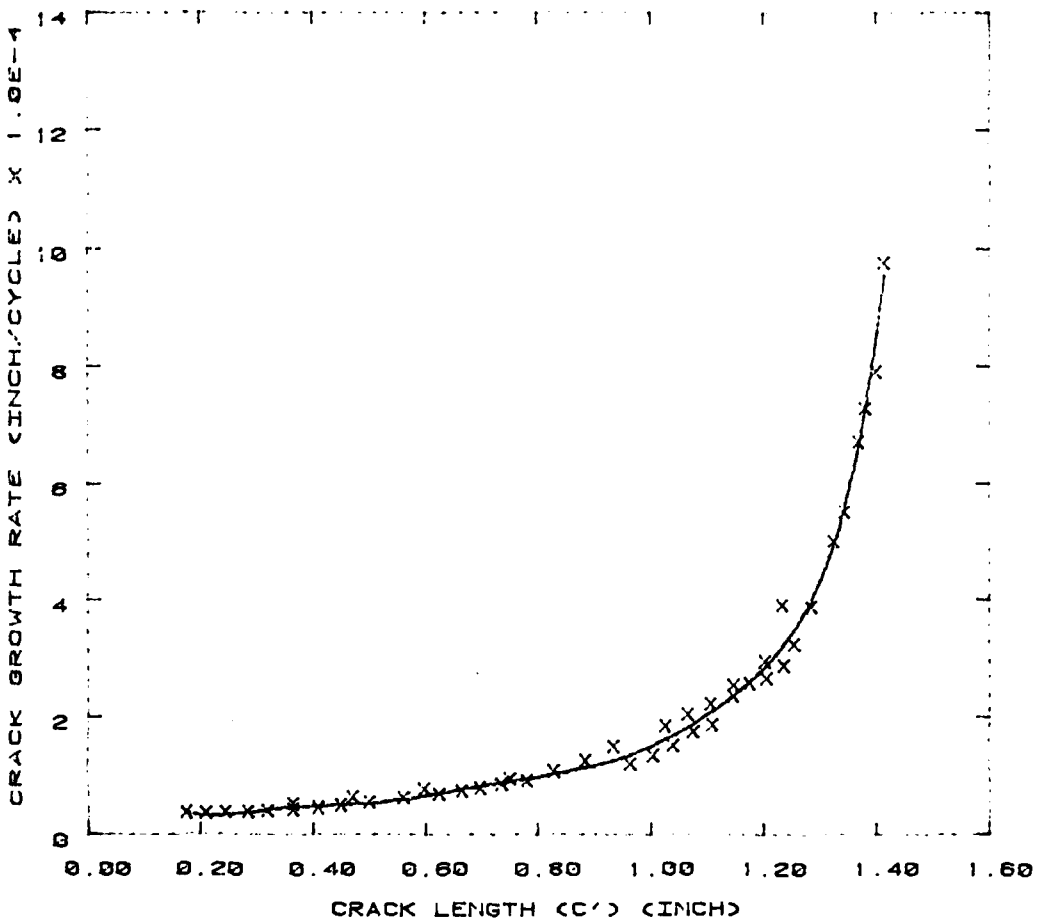

Figure A-5: Crack Growth Rate for the Back Surface of 7075-T651 Aluminum Specimens with a Maximum Stress of 15 and a Load Ratio of -0.3 as a Function of Crack Length

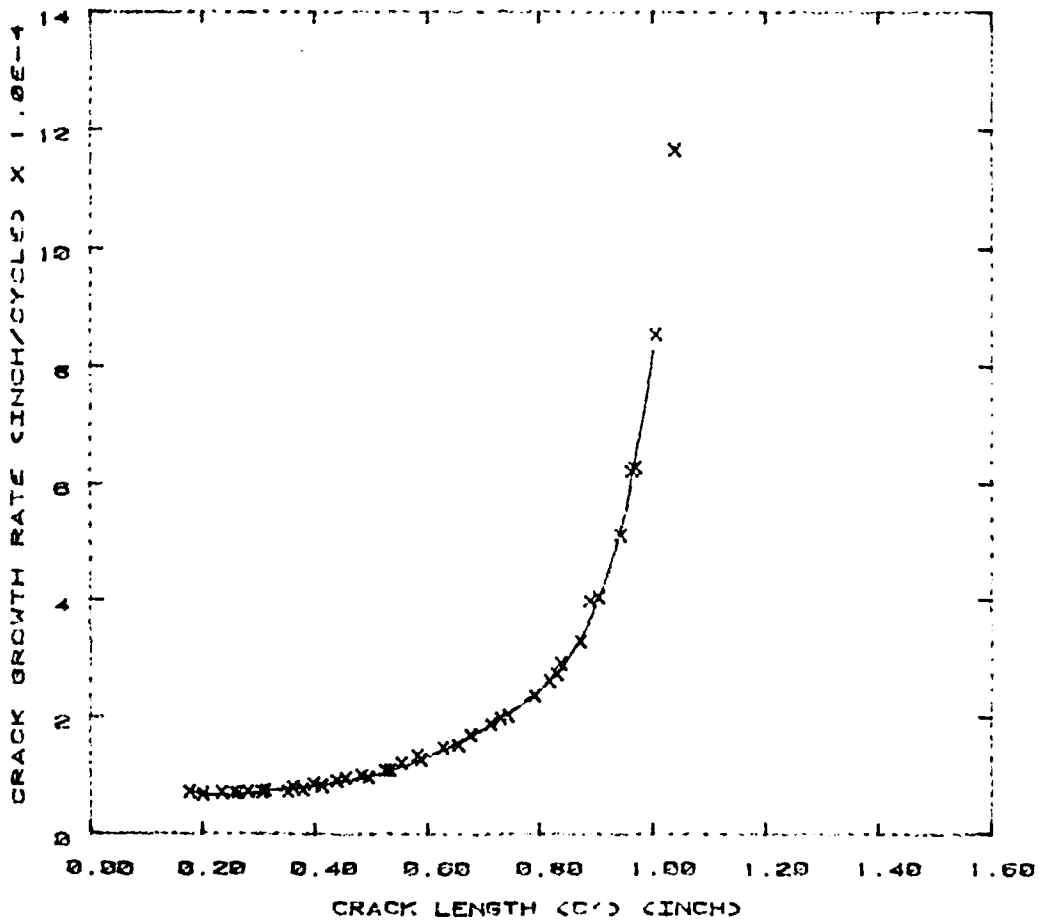

Figure A-6: Crack Growth Rate for the Back Surface of 7075-T651 Aluminum Specimens with a Maximum Stress of 20 and a Load Ratio of -0.5 as a Function of Crack Length

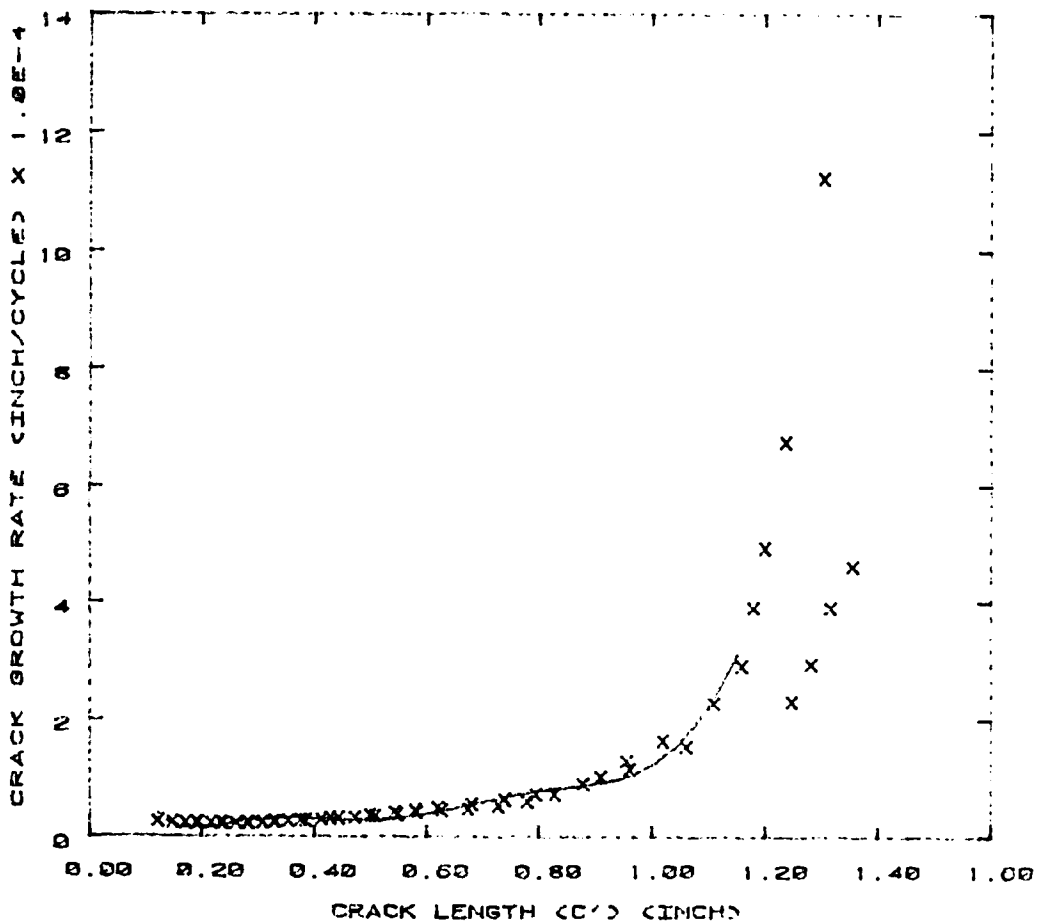

Figure A-7: Crack Growth Rate for the Back Surface of 7075-T651 Aluminum Specimens with a Maximum Stress of 15 and a Load Ratio of -0.5 as a Function of Crack Length

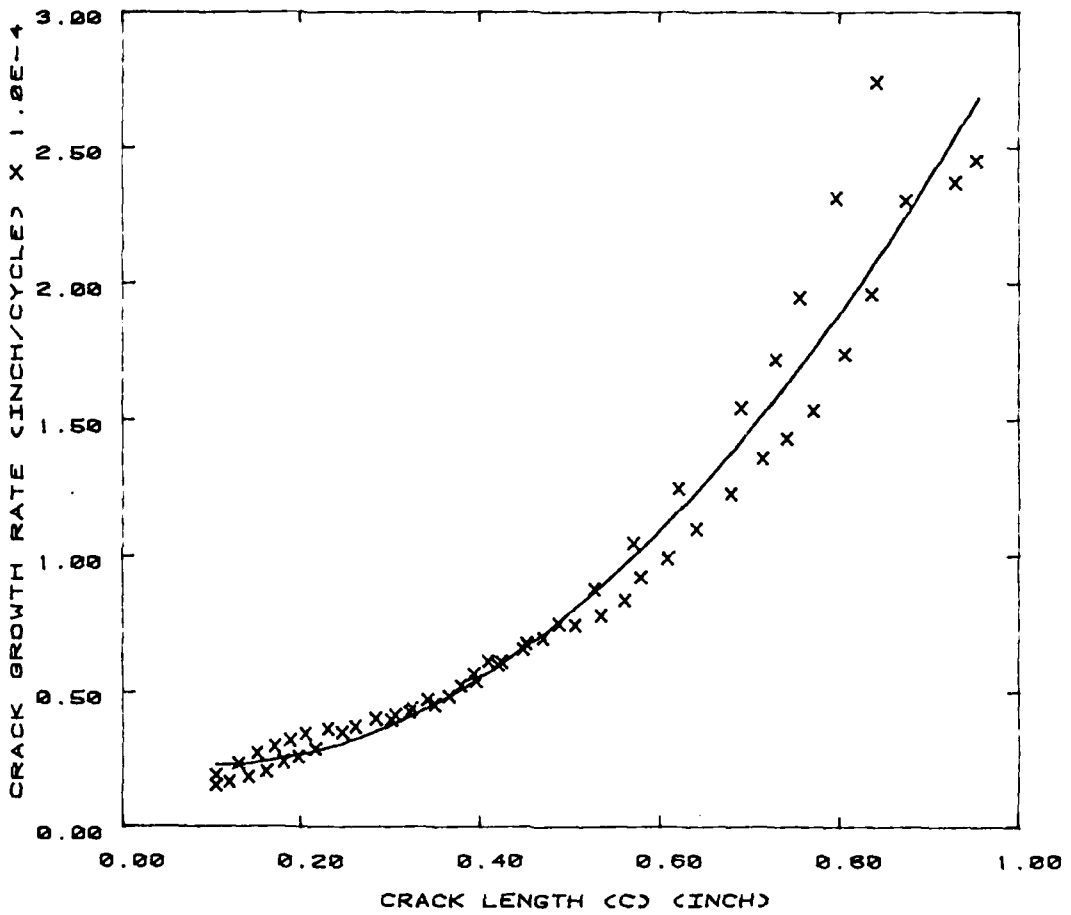

Figure A-8: Crack Growth Rate for the Front Surface of 7075-T651 Aluminum Specimens with a Maximum Stress of 20 and a Load Ratio of 0.1 as a Function of Crack Length

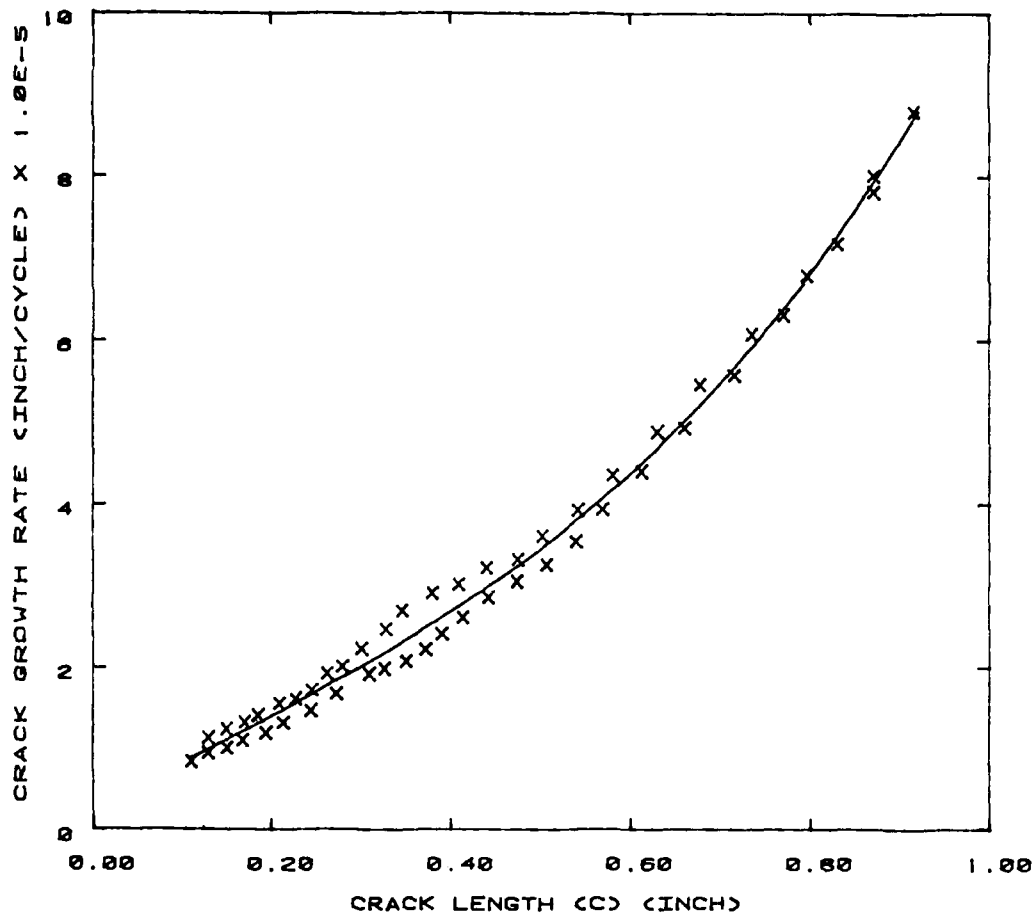

Figure A-9: Crack Growth Rate for the Front Surface of 7075-T651 Aluminum Specimens with a Maximum Stress of 15 and a Load Ratio of 0.1 as a Function of Crack Length

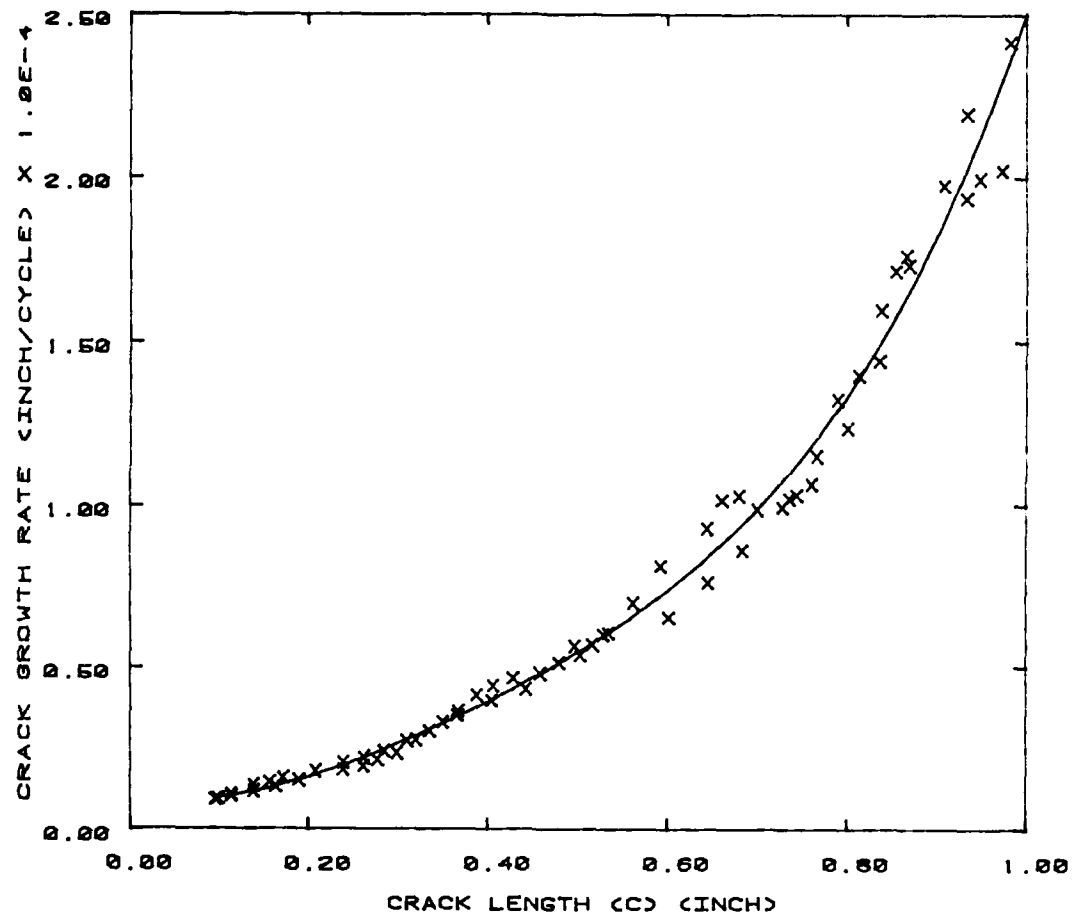

Figure A-10: Crack Growth Rate for the Front Surface of 7075-T651 Aluminum Specimens with a Maximum Stress of 20 and a Load Ratio of 0.3 as a Function of Crack Length

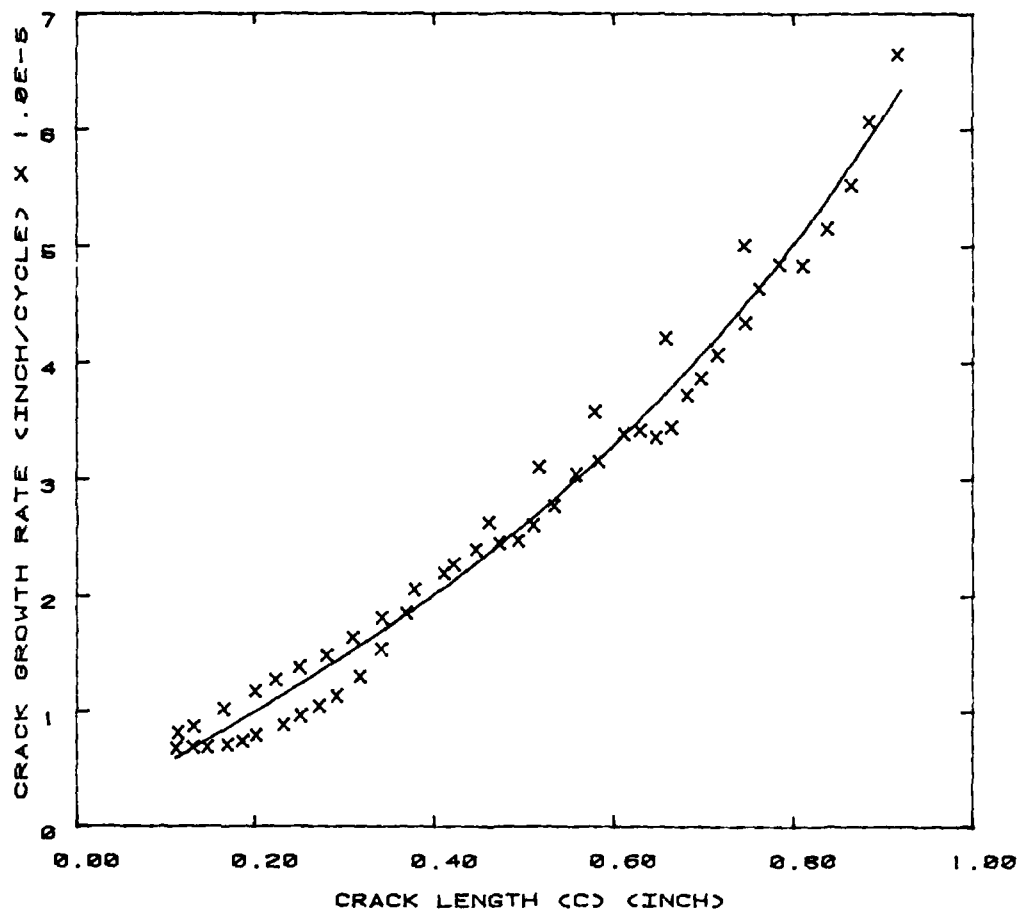

Figure A-11: Crack Growth Rate for the Front Surface of 7075-T651 Aluminum Specimens with a Maximum Stress of 15 and a Load Ratio of 0.3 as a Function of Crack Length

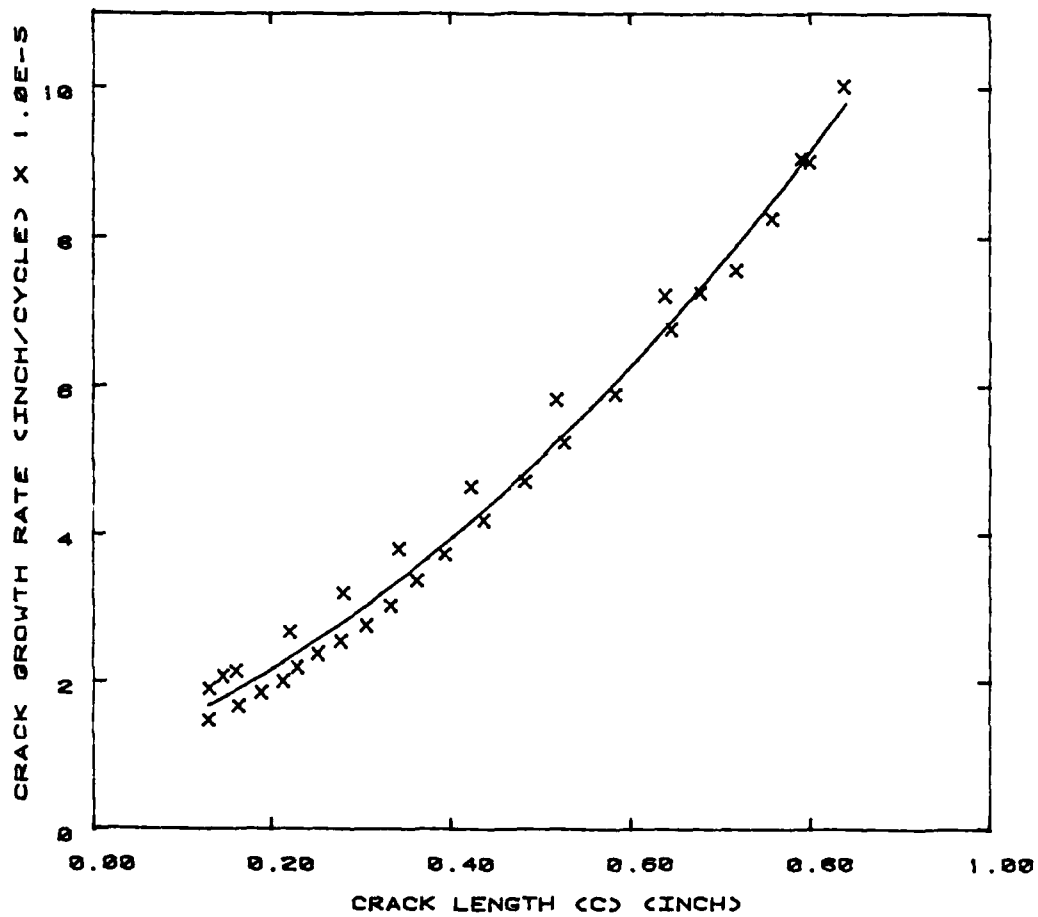

Figure A-12: Crack Growth Rate for the Front Surface of 7075-T651 Aluminum Specimens with a Maximum Stress of 15 and aLoad Ratio of -0.3 as a Function of Crack Length

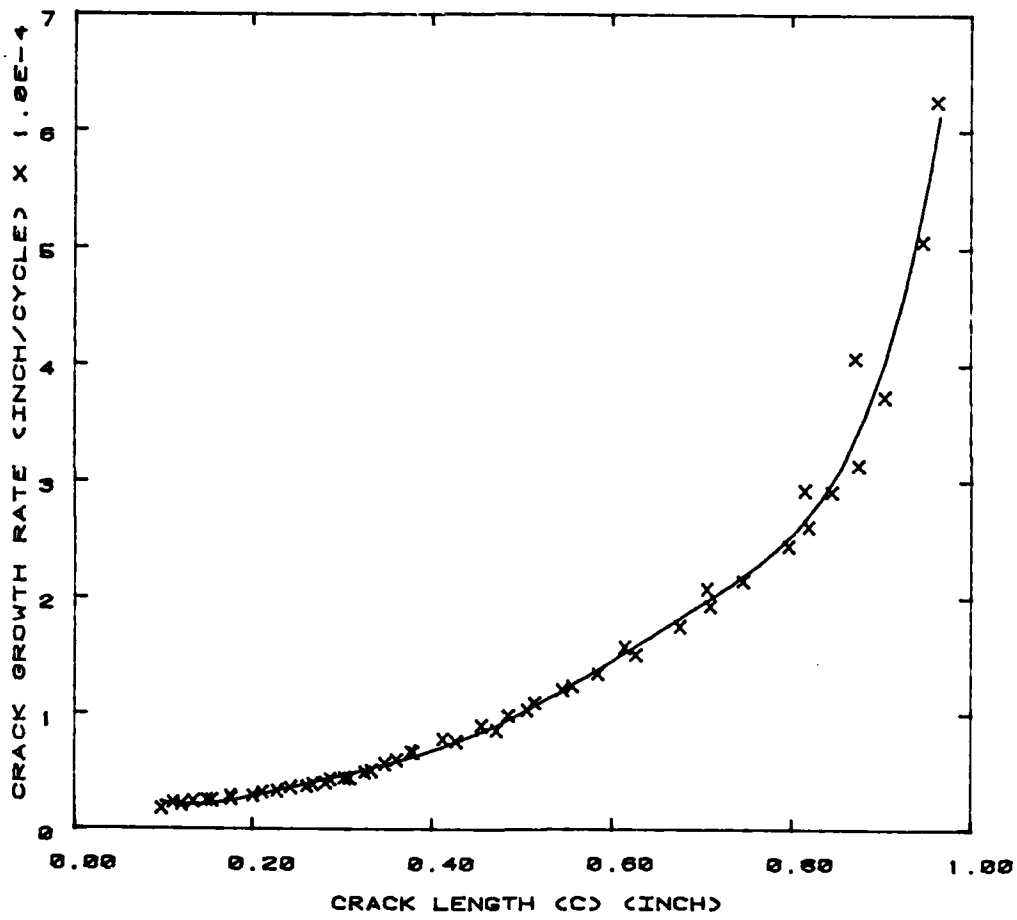

Figure A-13: Crack Growth Rate for the Front Surface of 7075-T651 Aluminum Specimens with a Maximum Stress of 20 and a Load Ratio of -0.5 as a Function of Crack Length

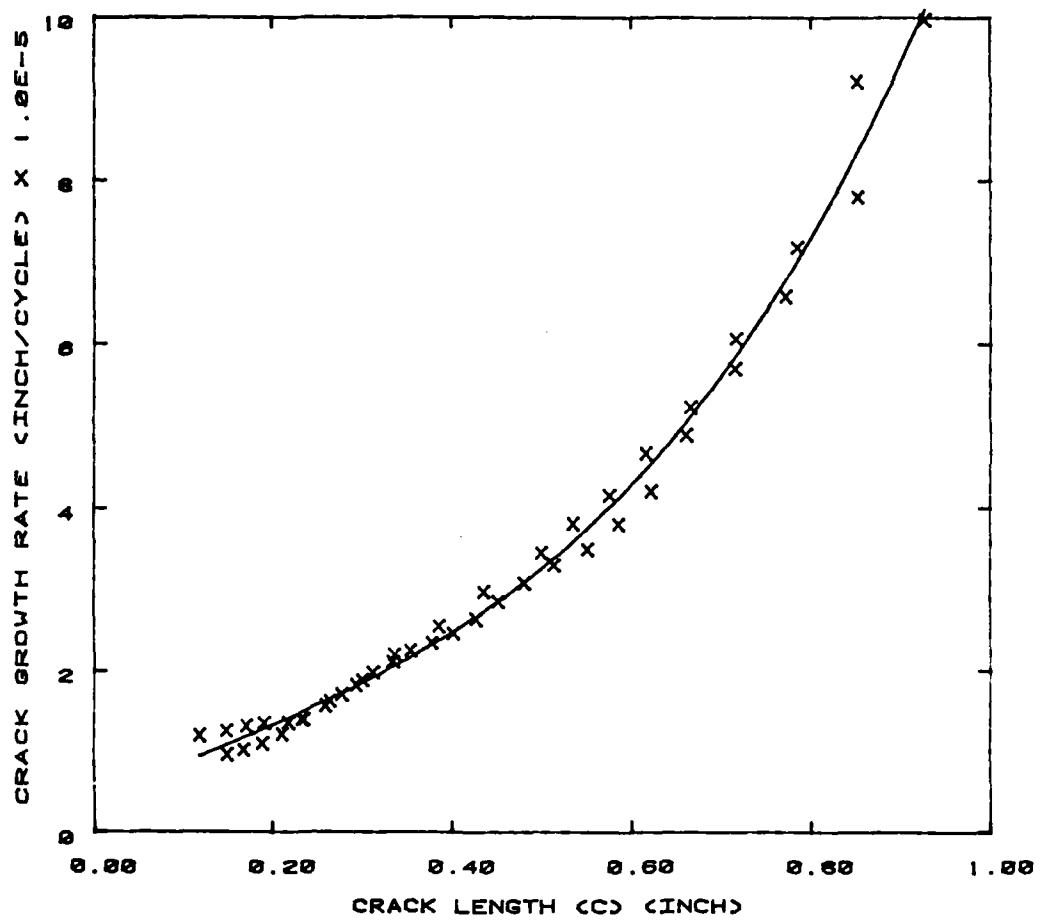

Figure A-14 Crack Growth Rate for the Front Surface of 7075-T651 Aluminum Specimens with a Maximum Stress of 15 and a Load Ratio of -0.5 as a Function of Crack Length

Bibliography

1. Gran, R.J., Orazio, F.D., Paris, P.C., Irwin, G.R. and Herzberg, R., "Investigation and Analysis Development of Early Life Aircraft Structural Failures," Technical Report AFFL-TR-70-149, Wright-Patterson AFB, Ohio, March 1971.

2. Wood, H.A. and Engle, R.M.,Jr., "Damage Tolerant Design Handbook, Guidelines for the Analysis and Design of Damage Tolerant Aircraft," Technical Report AFFDL-TR-79-3021, Wright-Patterson AFB, Ohio, March 1979.

3. Bowie, O.L., "Analysis of an Infinite Plate Containing Radial Cracks Originating at the Boundary of an Internal Circular Hole," Journal of Mathematics and Physics, Vol 35, 1956, pp 60-71.

4. Tweed, J. and Rooke, D.P., "The Distribution of Stress Near the Tip of a Radial Crack at the Edge of a Circular Hole," International Journal of Engineering Science, Vol 11, 1973, pp 1185-1195.

5. Kobayashi, A.S., "A Simple Procedure for Estimating Stress Intensity Factor in Region of High Stress Gradient," Significance of Defects in Welded Structures, Proceedings of the Japan-US Seminar, Tokyo,1973.

6. Liu, A.F., "Stress Intensity Factor for a Corner Flaw," Engineering Fracture Mechanics, Vol 4, 1972, pp 175-179.

7. Smith, F.W., Emery, A.F. and Kobayashi, A.S., "Stress Intensity Factors for Semicircular Cracks," Journal of Applied Mechanics, Vol 34, December 1967.

8. Kobayashi, A.S. and Moss, W.L., "Stress Intensity Magnification Factors for Surface-Flawed Tension Plate and Notched Round Tension Bar," Fracture 1969, Chapman and Hall, London, 1969.

9. Shah, R.C., "Stress Intensity Factors for Through and Part-Through Cracks Originating at Fastener Holes," Eighth National Symposium on Fracture Mechanics, Brown University, August 1974.

10. Shah, R.C. and Kobayashi, A.S., "Stress Intensity Factors for an Elliptical Crack Approaching the Surface of a Semi-Infinite Solid," International Journal of Fracture, Vol 9, No 2, 1973.

11. Grandt, A.F.,Jr., "Stress Intensity Factors for Some Thru-Cracked Fastener Holes," Seventh National Congress of Applied Mechanics, University of Colorado, June 1974.

12. Han, H.P. and Liu, A.F., "A Survey of Stress Intensity Equations for Corner Cracks at Holes," Report No NOR-77-112, Northrop Corporation, December 1977.

13. Isida, M., "Stress Intensity Factors for the Tension of an Eccentrically Cracked Strip," Transcript ASME, Series E, Journal of Applied Mechanics, Vol 33, 1965.

14. Newman, J.C.,Jr. and Raju, I.S., "Stress Intensity Factor Equations for Cracks in Three-Dimensional Finite Bodies," NASA Technical Memorandum 83200, National Aeronautics and Space Administration, August 1981.

15. Raju, I.S. and Newman, J.C.,Jr., "Stress Intensity Factors for a Wide Range of Semi-Elliptical Surface Cracks in Finite-Thickness Plates," Engineering Fracture Mechanics Journal, Vol 11, No 4, 1979, pp 817-829. (See also NASA TM X-72825, August 1977.)

16. Howland, R.C.J., "On the Stresses in the Neighbourhood of a Circular Hole in a Strip Under Tension," Philos. Trans. Royal Society London, Series A, Vol 229, January 1930, pp 49-86.

17. Tada, H., Paris, P.C. and Irwin, G.R., "The Stress Analysis of Cracks Hand-book," Del Research Corporation, 1973.

18. Irwin, G.R., "The Crack Extension Force for a Part-Through Crack in a Plate," ASME, Journal of Applied Mechanics, Vol 29, No 4, 1962, pp 651-654.

19. Smith, F.W. and Kullgren, T.E., "Theoretical and Experimental Analysis of Surface Cracks Emanating from Fastener Holes," Technical Report AFFDL-TR-76-104, Wright-Patterson AFB, Ohio, February 1977.

20. Heckel, J.B. and Rudd, J.L., "Assessment of Stress Intensity Factors for Corner Cracks at Holes," Technical Report AFWAL-TM-82-201-FIBE, Wright-Patterson AFB, Ohio, August 1982.

21. Chang, J.B., editor, Part-Through Crack Fatigue Life Prediction, ASTM STP 687, ASTM, Philadelphia, October 1979.

22. Vroman, G.A. and Peterson, D.E., "Computer-Aided Fracture Mechanics Life Prediction Analysis," ASTM STP 687, 1979, pp 129-142.

23. Kobayashi, A.S. and Moss, W.L., in Proceedings, Second International Conference on Fracture, Brighton, England, 1969, pp 31-45.

24. Johnson, W.S., "Prediction of Constant Amplitude Fatigue Crack Propagation in Surface Flaws," ASTM STP 687, 1979, pp 143-155.

25. Brussat, T.R. and Chiu, S.T., "Flaw Growth in Complex Structure," Technical Report AFFDL-TR-77-79, Vol 1, Wright-Patterson AFB, Ohio, September 1977.

26. Engle, R.M.,Jr., "CRACKS II User's Manual," Technical Report AFFDL-TM-74-173 , Wright-Patterson AFB, Ohio, July 1974.

27. Grandt, A.F. and Hinnerichs, T.D., "Stress Intensity Factor Measurements for Flawed Fastener Holes," Proceedings for the Army Symposium on Solid Mechanics, South Yarmouth, Cape Cod, Massachusetts, September 1974.

28. Grandt, A.F. and Snow, J.R., "A Stress Intensity Factor Calibration for Corner Flaws at an Open Hole," Technical Report AFML-TR-74-282, Wright-Patterson AFB, Ohio, May 1975.

29. Heckel, J.B. and Rudd, J.L., "Evaluation of Analytical Solutions for Corner Cracks at Holes," Sixteenth National Symposium on Fracture Mechanics, Columbus, Ohio, August 1983.

30. Grimsley, F.M., "Crack Rate Analysis and Walker Equation Solver Using the Method of Least Squares (CRAWLS)," Technical Report AFWAL-TM-82-151-FIBE, Wright-Patterson AFB, Ohio, November 1981.

31. James, L.A. and Anderson, W.E., "A Simple Experimental Procedure for Stress Intensity Calibration," Engineering Journal of Fracture Mechanics, Vol 1, No 3, April 1969, p 565.

VITA

Captain Stephen William Opel [redacted] He graduated from high school in Jasper, Indiana in 1973 and attended the United States Air Force Academy from which he received a Bachelor of Science degree in Engineering Mechanics in June 1977. He received a commission in the United States Air Force upon graduation. He completed missile training in December 1977 and then served as a Minuteman deputy commander, instructor, and evaluator in the 66th and 67th Strategic Missile Squadrons and the 44th Strategic Missile Wing, at Ellsworth Air Force Base, South Dakota. In June of 1982, he entered the Air Force Institute of Technology's School of Engineering.

[redacted]

UNCLASSIFIED
SECURITY CLASSIFICATION OF THIS PAGE

REPORT DOCUMENTATION PAGE

1a. REPORT SECURITY CLASSIFICATION UNCLASSIFIED	1b. RESTRICTIVE MARKINGS
2a. SECURITY CLASSIFICATION AUTHORITY	3. DISTRIBUTION/AVAILABILITY OF REPORT Approved for public release; distibution unlimited.
2b. DECLASSIFICATION/DOWNGRADING SCHEDULE	
4. PERFORMING ORGANIZATION REPORT NUMBER(S) AFIT/GAE/AA/83D-17	5. MONITORING ORGANIZATION REPORT NUMBER(S)
6a. NAME OF PERFORMING ORGANIZATION School of Engineering 6b. OFFICE SYMBOL (If applicable) AFIT/EN	7a. NAME OF MONITORING ORGANIZATION
6c. ADDRESS (City, State and ZIP Code) Wright-Patterson AFB, Ohio 45433	7b. ADDRESS (City, State and ZIP Code)
8a. NAME OF FUNDING/SPONSORING ORGANIZATION AF Wright Aeronautical Labs 8b. OFFICE SYMBOL (If applicable) FIBE	9. PROCUREMENT INSTRUMENT IDENTIFICATION NUMBER
8c. ADDRESS (City, State and ZIP Code) Wright-Patterson AFB, Ohio 45433	10. SOURCE OF FUNDING NOS. PROGRAM ELEMENT NO. / PROJECT NO. / TASK NO. / WORK UNIT NO.
11. TITLE (Include Security Classification) See Box 19.	
12. PERSONAL AUTHOR(S) Stephen W. Opel, Captain, USAF	
13a. TYPE OF REPORT MS Thesis 13b. TIME COVERED FROM _____ TO _____	14. DATE OF REPORT (Yr., Mo., Day) 83 Dec 15. PAGE COUNT 104
16. SUPPLEMENTARY NOTATION Approved for public release; IAW AFR 190-17. LYNN E. WOLAVER Dean for Research and Professional Development Air Force Institute of Technology (ATC) Wright-Patterson AFB, OH 45433 3 JAN 1984	

17. COSATI CODES			18. SUBJECT TERMS (Continue on reverse if necessary and identify by block number)
FIELD	GROUP	SUB. GR.	Stress Intensity Factor
20	11		Corner-Crack-at-a-Hole
			Transition

19. ABSTRACT (Continue on reverse if necessary and identify by block number)

Title: TRANSITION OF CORNER CRACKS AT HOLES INTO THROUGH-THE-THICKNESS CRACKS

Thesis Chairman: George K. Haritos, Major, USAF

20. DISTRIBUTION/AVAILABILITY OF ABSTRACT UNCLASSIFIED/UNLIMITED ☒ SAME AS RPT. ☐ DTIC USERS ☐	21. ABSTRACT SECURITY CLASSIFICATION UNCLASSIFIED
22a. NAME OF RESPONSIBLE INDIVIDUAL George K. Haritos, Major, USAF	22b. TELEPHONE NUMBER (Include Area Code) 513-255-3517 22c. OFFICE SYMBOL AFIT/ENY

DD FORM 1473, 83 APR EDITION OF 1 JAN 73 IS OBSOLETE.

UNCLASSIFIED
SECURITY CLASSIFICATION OF THIS PAGE

This study developed correction factors for currently used stress intensity factor equations to more accurately predict stress intensity factors for a corner crack emanating from a hole as it transitions to a uniform through-the-thickness crack. These correction factors resulted in an approximate 15 percent increase in total life prediction and a far better correlation between analytical stress intensity factor predictions and experimental results in the transition region. The material used for total life predictions was 7075-T651 Aluminum, and the initial crack eccentricity, a/c, was always greater than one.

Correlations were accomplished between experimental results from Polymethylmethacrylate (PMMA) testing and the Newman-Raju three-dimensional stress intensity factor equation for a single corner crack at a hole where the crack eccentricity is greater than one. These correlations were plotted from crack initiation until back surface penetration for both the top surface and along the bore of the hole. From these plots correction factors were determined and a transition starting point was located. The transition region begins when the normalized crack depth reaches 0.75.

Correlations were also accomplished between experimental results from 7075-T651 Aluminum testing and the Grandt linearization of the Bowie equation for a through-crack emanating from a hole. These correlations were plotted from back surface penetration to final fracture. The plot yields the end of the transition region, and also the required correction factors to be utilized. The transition region ends when the normalized crack length reaches 2.5.

Life predictions were then made using the corrected model, Engle's model, (which includes the Newman-Raju equation and Grandt's linearization of the Bowie equation), and Brussät's model. The corrected model produced better predictions than the Engle model in total life,and in predicting life from back surface penetration to final fracture for constant amplitude loading. The corrected model yields a slightly more conservative crack shape and life prediction from crack initiation until back surface penetration than the Engle model.